

Modelling root exudation and plant-microbe interactions under CO₂ fertilization in a mature forest

Kristian Schufft^{1,2,3}, Katrin Fleischer⁴, Anja Rammig³, Lin Yu⁵, Mingkai Jiang⁶, Belinda E. Medlyn⁷, Sönke Zaehle^{1,8}

5 ¹ Department Biogeochemical Signals, Max Planck Institute for Biogeochemistry, Jena, Germany

² International Max Planck Research School for Global Biogeochemical Cycles, Max Planck Institute for Biogeochemistry, Jena, Germany

³ Technical University of Munich, School of Life Sciences, Freising, Germany

10 ⁴ Systems Ecology, Amsterdam Institute for Life and Environment, Vrije Universiteit Amsterdam, Amsterdam, The Netherlands

⁵ Department of Earth System Sciences, Hamburg University, Hamburg, Germany

⁶ State Key Laboratory for Vegetation Structure, Function and Construction (VegLab), College of Life Sciences, Zhejiang University, Hangzhou, Zhejiang, China, 310030

⁷ Hawkesbury Institute for the Environment, Western Sydney University, Penrith NSW Australia

15 ⁸ Michael Stifel Center Jena for Data-driven and Simulation Science, Friedrich Schiller University Jena, Jena, Germany

Correspondence to: Kristian Schufft (kschufft@bgc-jena.mpg.de)

Abstract. Root exudation, defined as plant labile carbon (C) allocation from fine roots into soils, is a substantial yet often overlooked pathway of the terrestrial C cycle. Root exudation is expected to increase under rising atmospheric CO₂, yet its consequences for soil C and nutrient cycling remain poorly constrained. Additional labile C input may stimulate microbial growth and increase soil C storage, but microbial nutrient acquisition could offset this through enhanced decomposition of soil organic matter.

Here, we implement a dynamic representation of root exudation, driven by plant surplus C and nutrient limitation, in the microbial-explicit terrestrial biosphere model QUINCY-JSM. We evaluate the effects of elevated CO₂ (eCO₂) on root exudation and on microbial C, nitrogen (N), and phosphorus (P) cycling using observations from the Eucalyptus Free Air CO₂ Enrichment (EucFACE) experiment in a soil P-impooverished forest. In this experiment, eCO₂ increased gross primary productivity (GPP) and soil respiration, but more than half of additional GPP under eCO₂ could not be assigned to measured biomass production or autotrophic respiration, and was likely allocated belowground.

With the explicit implementation of root exudation, the model predicted that eCO₂ increases belowground C allocation by 20% and microbial growth by 14%, but has a limited effect on soil C storage. Root exudation increased by 30%, but more than half of this additional input was directly respired by microbes. Thus, root exudation gives a possible explanation for the unmeasured fraction of plant C allocation, effectively closing the gap between enhanced GPP and increased heterotrophic respiration under eCO₂ in the experiment. Although increased C input through root exudation stimulated microbial growth, microbes partially met their higher nutrient demand through a 9% higher decomposition and increased mineralization of organic matter, which negated the build-up of microbial necromass. Our study highlights the importance of root exudation as a key pathway in vegetation C allocation under eCO₂ and identifies microbial responses to this flux as a key modulator of soil C sequestration in nutrient-limited forests, thereby guiding further research regarding plant-microbe interactions.

Short summary. Root exudation describes a process in which plants allocate labile carbon (C) through roots into soils, thereby influencing microbial C and nutrient cycling. We implemented root exudation in a computer model that simulates ecosystem processes. Increased atmospheric CO₂ increased root exudation, but the additional input was partially offset by enhanced microbial respiration. Our research brings new perspectives in modelling soil C and nutrient cycling in forests under increasing CO₂.

45

1. Introduction

Increasing atmospheric CO₂ concentrations have the potential to drive increased ecosystem carbon (C) sequestration, but there is considerable uncertainty about how much additional C can be stored in ecosystems, particularly where soil nutrient availability is low. ~~Observation and modeling studies suggest, that CO₂ fertilization leads to higher leaf level photosynthesis and biomass production (BP) (Norby, 2025; Walker et al., 2019, 2021),~~ Observation and modeling studies suggest that CO₂ fertilization leads to higher leaf-level photosynthesis and biomass production (BP), defined as the use of photosynthates for plant growth, potentially increasing C sequestration in vegetation biomass, and in soils when vegetation biomass ~~turn over.~~ ~~However, increased growth must be supported by nutrients~~ turns over (Norby, 2025; Walker et al., 2019, 2021). ~~However,~~ increased growth must be supported by nutrients, and if soil nutrient availability cannot meet increased plant nutrient demands, the CO₂ fertilization effect on plant growth is typically reduced (Fleischer et al., 2019; Norby et al., 2010; Wieder et al., 2015; Zaehle et al., 2014). Under elevated ~~CO₂~~ eCO₂ (eCO₂), plants may allocate additional C derived from increased photosynthesis to root exudation and mycorrhizae to compensate for nutrient limitations, by increasing microbial decomposition and mineralization of organic matter (Drake et al., 2011; Phillips et al., 2011; Reay et al., 2025). Observations and models suggest that root exudation is a key mechanism for plant responses under eCO₂, but there are major uncertainties about microbial responses and the consequences on soil C sequestration, especially for different natures of nutrient limitations.

Free Air Carbon Enrichment (FACE) experiments in nitrogen (N) limited forests suggest increased root exudation and cycling of soil organic matter helped ~~in maintaining to sustain a positive~~ BP response to eCO₂. In Duke FACE and ORNL FACE, which were located in temperate N-limited forests, eCO₂ has led to an initial increase in BP. However, only at Duke FACE, eCO₂ increased N uptake and a change in plant nitrogen-use efficiency allowed for a sustained response in BP to eCO₂, while in ORNL FACE progressive N limitation decreased the positive response of BP under eCO₂ after 10 years (Norby et al., 2010; Walker et al., 2019; Zaehle et al., 2014). One explanation is that plants maintained N availability under eCO₂ at Duke FACE, by promoting enhanced decomposition of soil organic matter (SOM) via increased root exudation, thereby increasing N mineralization but offsetting accumulation of C in soil pools (Drake et al., 2011; Terrer et al., 2021).

~~Synthesis-Model-data synthesis~~ of observations from FACE experiments and terrestrial biosphere models (TBMs) highlighted the role of plant-soil interactions but also revealed model limitations. ~~Model data synthesis identified C allocation, N uptake and soil N cycling as key processes for CO₂ responses under N limitation~~ (De Kauwe et al., 2014; Zaehle et al., 2014). These studies identified C allocation, N uptake, and soil N cycling as key processes for CO₂ responses under N limitation. However, most models were unable to fully reproduce the dissimilar responses to eCO₂ under N limitation. While models reproduced the initial increase in BP, they generally tended to show a decreased response in BP due to progressing N limitation. This suggests a missing link between plant C allocation and nutrient acquisition, and highlights the importance ~~for~~ of root exudation in plant responses to eCO₂ in N-limited forests. However, it is not clear how additional root exudation under eCO₂ controls

80 microbial growth and soil C sequestration, and if results for N-limited forests can be transferred to phosphorus (P) limited systems.

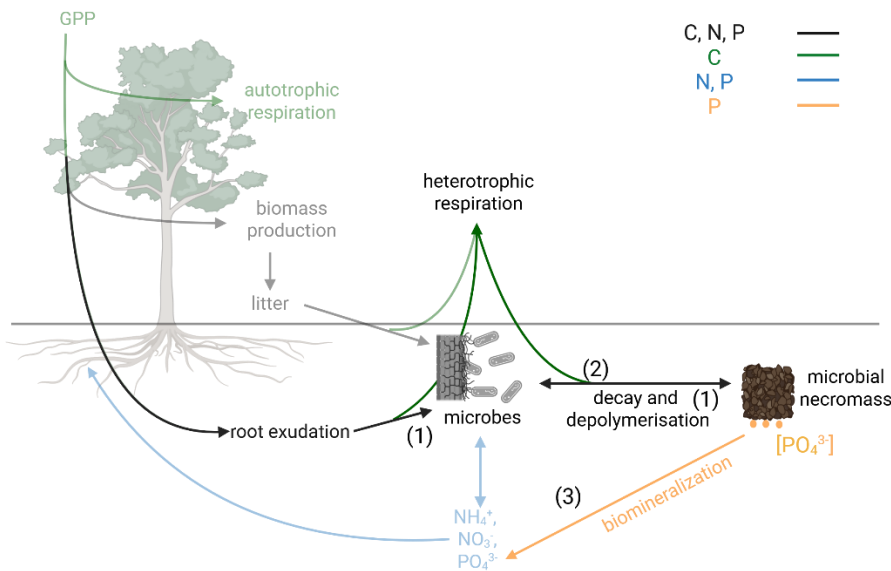
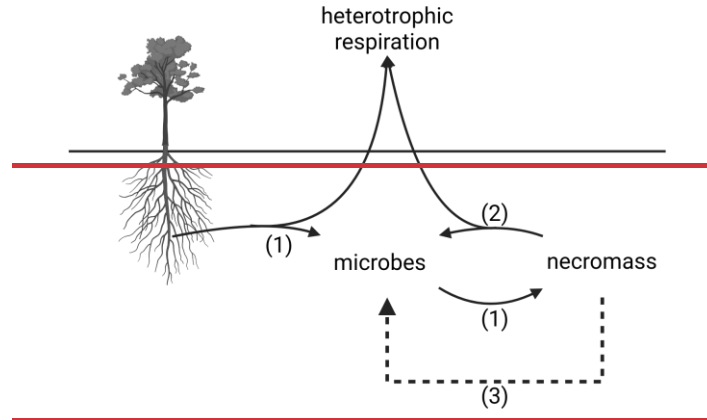
85 Despite the fact that P limitation is widespread globally (Du et al., 2020), previous forest FACE experiments have been principally conducted in N-limited temperate forests. The Eucalyptus Free Air CO₂ Enrichment (EucFACE) facility (Crous et al., 2015; Ellsworth et al., 2017) is the first large-scale FACE experiment investigating the impact of eCO₂ on forest ecosystems under P limitation. At the site eCO₂ increased gross primary productivity (GPP) by 12%, but the effect on biomass production and autotrophic respiration was comparatively small (Jiang et al., 2020). Notably, Jiang et al. (2020) found that more than 50% of additional GPP under eCO₂ could not be attributed to biomass production or autotrophic respiration; in this experiment. Instead, this C was traced to ~~an~~ a 17% increase in heterotrophic soil respiration, without a statistically significant increase in soil C sequestration. The results suggest that increased root exudation and induced cycling of SOM are also relevant for P-limited systems under eCO₂ (De Andrade et al., 2022; Lambers, 2022; Reichert et al., 2022; Wang and Lambers, 2020). However, the plant-microbial mechanisms ~~which that~~ link increased GPP with soil respiration, and ~~its the~~ implication for soil C sequestration in this system, remain poorly understood.

95 Similar to model-data synthesis for N-limited ~~forest forests~~, model-data synthesis for EucFACE identified nutrient limitation and C allocation as key mechanisms for understanding BP and soil activity response to eCO₂. Medlyn et al. (2016) found that in models with ~~an~~ integrated P cycle, under eCO₂ plant uptake remained unchanged, preventing a strong ~~increase in BP in~~ response ~~in BP~~ to eCO₂, whereas in other models eCO₂ increased BP up to 20%. Jiang et al. (2024a) compared 8 TBMs to the experimental results of EucFACE, and further pointed to the lack of adequate representation of plant C allocation. Most models allocated additional plant C ~~into~~ either autotrophic respiration, growth, or storage but not ~~into~~ heterotrophic respiration. This disagrees with C budget results from (Jiang et al., (2020) and indicates a missing representation of root exudation and plant-microbe interactions in these models, therefore neglecting possible ~~implication~~ implications for soil C storage under eCO₂.

105 Here, we aim to address the key missing link between GPP increase, plant C allocation and cycling of C, N, and P in soils by implementing root exudation in the microbial-explicit, terrestrial biosphere model, QUINCY-JSM (Thum et al., 2019; Yu et al., 2020) to simulate CO₂ fertilization at EucFACE. Like in other models, previous simulations with QUINCY-JSM, showed a mismatch between simulated and observed C allocation and response of soil heterotrophic respiration to eCO₂ for EucFACE (Jiang et al., 2020). We therefore implemented root exudation in QUINCY-JSM. We ~~assume model~~ root exudation as a dynamic flux, based on plant fine root respiration and nutrient status. We use our model to investigate how root exudation affects underlying mechanisms of microbial soil C sequestration under eCO₂.

Microbes fulfill a central role in soil C sequestration, by decomposing and respiring organic material, controlling nutrient release and contributing to organic matter formation and long-term C sequestration, via production of necromass and ~~the~~ formation of organo-mineral associations (Kästner et al., 2021; Liang et al., 2017, 2019; Sokol et al., 2019). Observational data alone may not be sufficient to disentangle contributions of individual processes. Therefore, we use our model to investigate three competing mechanisms that may regulate soil C sequestration response in microbial necromass to altered microbial growth and nutrient acquisition as a result of increased root exudation (Figure 1).

- (1) Exudates regulate gross growth of microbial biomass, which in turn influences gross necromass production (Figure 1 (1)) (Cotrufo et al., 2013). The capability of microbes to transform additional soil C input into biomass depends on their carbon-use efficiency (CUE). ~~Carbon~~The carbon-use efficiency of microbial growth has been shown to be constrained under nutrient limitations (Manzoni et al., 2012; Spohn, 2015). If microbes are not able to fulfill their stoichiometric nutrient requirement for growth, excess C will be respired as “waste” respiration, leading to a decline in microbial growth CUE (Schimel and Weintraub, 2003). How much of the additional C input is ultimately transferred into biomass and necromass therefore depends on microbial nutrient limitation.
- (2) Under N or P limitation, microbes can stimulate the depolymerisation of nutrient-rich microbial necromass to potentially acquire more N and P (Figure 1 (2)) (van Groenigen et al., 2014; Vestergård et al., 2016; Yin et al., 2013). While this may happen ~~proportional~~proportionally to growth, microbes may also change their relative investment into nutrient acquisition strategies. Either way, the additional depolymerization of microbial necromass under increased root exudation, often referred to as priming, will result in an increased respiration of old organic C and has the potential to offset the gross growth of necromass.
- (3) Under strong P limitation, P can be gained through biochemical mineralization without the need to decompose necromass (Figure 1 (3)) (Margalef et al., 2017; Turner et al., 2014; Walker and Syers, 1976). In this process, microbes use phosphatase to hydrolyze terminal phosphate groups from organic matter as inorganic PO₄ that is available for plants and microbes (McGill and Cole, 1981; Nannipieri et al., 2011). As this mechanism does not require the full depolymerization of microbial necromass, it decouples microbial nutrient acquisition from C cycling and does not directly decrease C storage.



150

Figure 1: Conceptual diagram of **microbial contributions of ecosystem processes related to soil organic matter formation**. (1) **plant** litter and exudates support microbial growth and necromass production, mediated by microbial CUE. (2) Microbes decompose microbial necromass for nutrient acquisition. (3) Biochemical mineralization allows for **P**-acquisition of **terminal phosphate** from microbial necromass without decomposition. **Black, solid arrows represent fluxes of C, N and P. Green, solid arrows represent C-only fluxes. Blue, solid arrows represent N and P fluxes. Yellow arrows refer to P-only fluxes.** Created with BioRender.com

155

With this study, we aim for a first quantification of root exudation fluxes for the EucFACE experiment. We test our implementation against observations [at EucFACE](#) regarding allocation of additional GPP under eCO₂ in the ecosystem. We further aim to answer the following ~~objectives~~ research questions:

- 160 (1) To ~~which~~ what extent did increased root exudation under eCO₂ contribute to gross microbial growth, gross necromass production, and increased heterotrophic respiration?
- (2) Was priming, as a mechanism for microbial N acquisition, increased by higher root exudation under eCO₂?
- (3) Was biochemical mineralization, as a mechanism for microbial P acquisition, increased by higher root exudation under eCO₂?
- 165 (4) Was net necromass production, defined as the difference between gross necromass production and decomposition, increased by higher root exudation under eCO₂?

We conclude our study by presenting key aspects in which linking models with field measurements can be used to further improve understanding of plant-microbe interactions under increasing levels of CO₂.

170 2. Material and Methods

2.1 Model application

We apply our model, QUINCY-JSM, to the Eucalyptus Free Air CO₂ Enrichment (EucFACE) experiment. Our goal is to quantify competing soil mechanisms on C storage for increased root exudation under eCO₂ in a P-limited forest. Therefore, we implemented root exudation, based on plant labile pool dynamics, in ~~our~~the model. We parameterize and apply our model to the EucFACE experiment (Crous et al., 2015; Ellsworth et al., 2017). We first evaluate our model against field measurements for ambient (aCO₂) conditions, then evaluate our results against measured CO₂ responses of plant C allocation to see if our model can simulate the suggested increase in root exudation under eCO₂. We further quantify the simulated increase in belowground C allocation and its effect on gross microbial growth. To assess feedback via microbial nutrient acquisition strategies we identify sources for gross microbial growth in C, N₂ and P and potential shifts in sources with eCO₂. We conclude by comparing simulated influx and outflux of microbial necromass C, N₂ and P pools and their turnover rates, for aCO₂ and eCO₂ conditions. QUINCY-JSM has two components, a terrestrial biosphere model (QUINCY (QUantifying Interactions between terrestrial Nutrient CYcles and the climate system; (Thum et al., 2019)) coupled to the integrated JSM (Jena Soil Model; (Yu et al., 2020)) and simulates coupled ecosystem N, P, C₂ and water dynamics (Figure 2 for an overview). In the following sections, we first summarize key processes represented in QUINCY and JSM, before introducing the new root exudation module.

2.2 Overview of modelled processes in QUINCY

QUINCY simulates the function of vegetation, which is described by five structural pools (leaves, fine roots, coarse roots, sapwood₂ and heartwood) and three non-structural pools (labile, storage₂ and fruits) that all contain C, N, and P. Photosynthesis is calculated after Friend and Kiang (2005) along a vertical canopy gradient (Kull and Kruijt, 1998), with photosynthetic activity assumed proportional to leaf N content, but attenuated in the presence of sink limitation on growth (Thum et al., 2019). Acquired C is added to the labile pool, from which it is used to cover the cost ~~for~~of respiration. Maintenance respiration is calculated for each tissue based on tissue N content and temperature (Lloyd and Taylor, 1994). In addition, QUINCY accounts for growth respiration (Atkin et al., 2014) and nutrient uptake respiration (Zerihun et al., 1998). The remaining C in the labile pool is then used for root exudation, growth, storage (Figure 2₂ upper panel). Nitrogen and P taken up by plant roots₂ or recycled from senescing tissues are added to the labile pool. Excess labile C, N₂ and P are stored in a reserve pool, from ~~where~~which these elements can be retrieved to buffer low levels of the labile pool, e.g., to ensure the regrowth of foliage and roots, root exudation (Sect. 2.4) and structural components at the start of the growing season. Upon senescence of structural pools, a fixed fraction of nutrients is recycled and returned into the labile pool. The remaining biomass (C, N, P) enters the soil via litterfall in the form of three litter pools (soluble, polymeric, wood). Vegetation and soil processes are calculated at a 30 min time-step. All physical and biogeochemical soil processes are modelled for 15 discrete soil layers, with exponentially increasing depth

and a minimum layer depth of 6.5 cm. The model accounts for differences in vegetation by twelve plant functional types (PFTs), of which for this study we use only the dry broadleaved evergreen type to represent vegetation at the site.

2.3 Overview of modelled processes in JSM

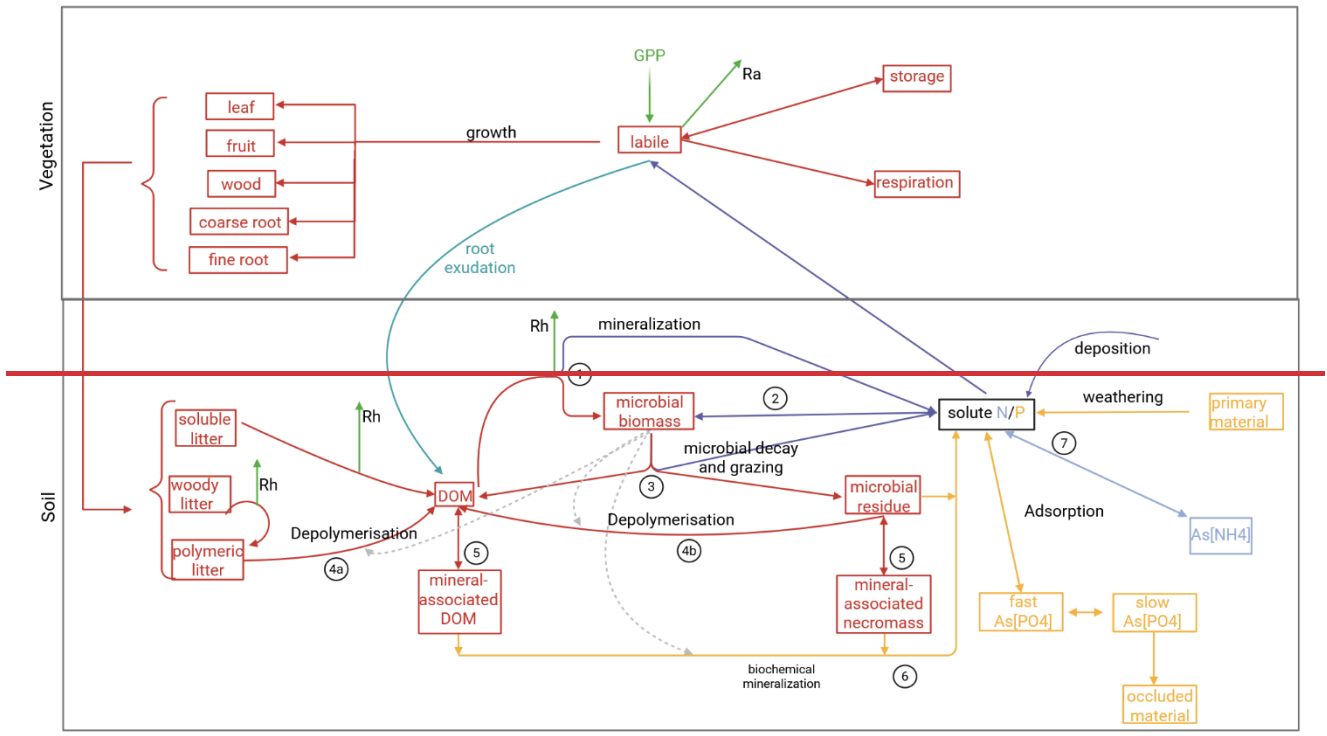
205 Soil biogeochemistry is modelled by a microbially explicit and vertically resolved SOM model (JSM; (Yu et al., 2020); Figure 2, lower panel, ~~Tab.~~ Table 1). All biogeochemical soil pools and processes are modelled for 15 discrete soil layers, along a vertical soil gradient. Soil layer thickness increases exponentially with depth. JSM considers five different SOM pools: dissolved organic matter (DOM), microbial biomass, microbial necromass, and organo-mineral-associated DOM and microbial necromass (Table 1). Depolymerization, DOM uptake and associated biological nutrient mineralization, and inorganic ~~nutrients~~nutrient uptake are affected by the abundance of microbial biomass, either modelled by using forward 210 Michaelis-Menten or reverse Michaelis-Menten kinetics (Schimel and Weintraub, 2003). Microbes take up C from DOM (Fig. 2, process 1). Nutrients are acquired from DOM or by immobilization of soluble nutrients (Fig. 2, process 2). DOM taken by microbes either enters microbial biomass or becomes mineralized, based on element-specific use-efficiencies. ~~Carbon~~The carbon-use efficiency of the microbial biomass varies as a function of nutrient availability between 30-% and 50-%, mimicking a change in microbial decomposer community. Mineralized C is emitted from soil as heterotrophic respiration. Soil organic 215 matter and inorganic forms of nutrients are transported between soil layers via water transport (for nutrients and dissolved organic matter) and bioturbation. Microbial decay is modelled as first-order decay with a constant turnover time of ~150 days. Dead microbial biomass is partitioned into DOM and microbial necromass, ~~corresponding to microbial necromass~~ (Fig. 2, process 3). The fraction of N and P entering DOM is higher than for C, to represent the lower C-to-nutrient ratio in cytoplasm (Schimel and Weintraub, 2003). Additionally, a constant fraction of N is transferred into inorganic soluble pools to mimic 220 grazing on living microbial biomass (Wutzler et al., 2022) (Eq. A1 to A5, Table A2). Decomposition of soluble and woody litter follows first-order decay, whereas the depolymerization of polymeric litter (Fig. 2, process 4a) and microbial necromass (Fig. 2, process 4b) into DOM is a function of microbial biomass pool and in addition, varying enzyme allocation based on microbial nutrient status (Wutzler et al., 2017; Yu et al., 2020). Organo-mineral-associated DOM and necromass ~~pool~~are protected from depolymerisation, but are exchanged with the 'free' DOM/~~necromass~~ pool via first-order sorption kinetics 225 (Fig. 2, process 5). Soil solution NH_4 and PO_4 are in adsorption/desorption interaction with soil surfaces, simulated by Langmuir equilibrium (Yu et al., 2023). Adsorption, plant uptake and microbial uptake of soluble nutrients are in direct competition with each other (Tang and Riley, 2013). In addition to biological nutrient mineralization that results from microbial DOM uptake, PO_4 is further mobilized through biochemical mineralization via acid phosphatase (Fig. 2, process 6). Biochemical mineralization is regulated by the production of phosphatase, which is assumed to be affected by root and 230 microbial biomass, as well as the C allocation for ~~productions~~production of other enzymes. This process allows for an additional pathway of access to P from microbial necromass and both organo-mineral-associated pools that cannot be directly depolymerised. As biochemical mineralization does not need complete decomposition of organic substances, it can affect the

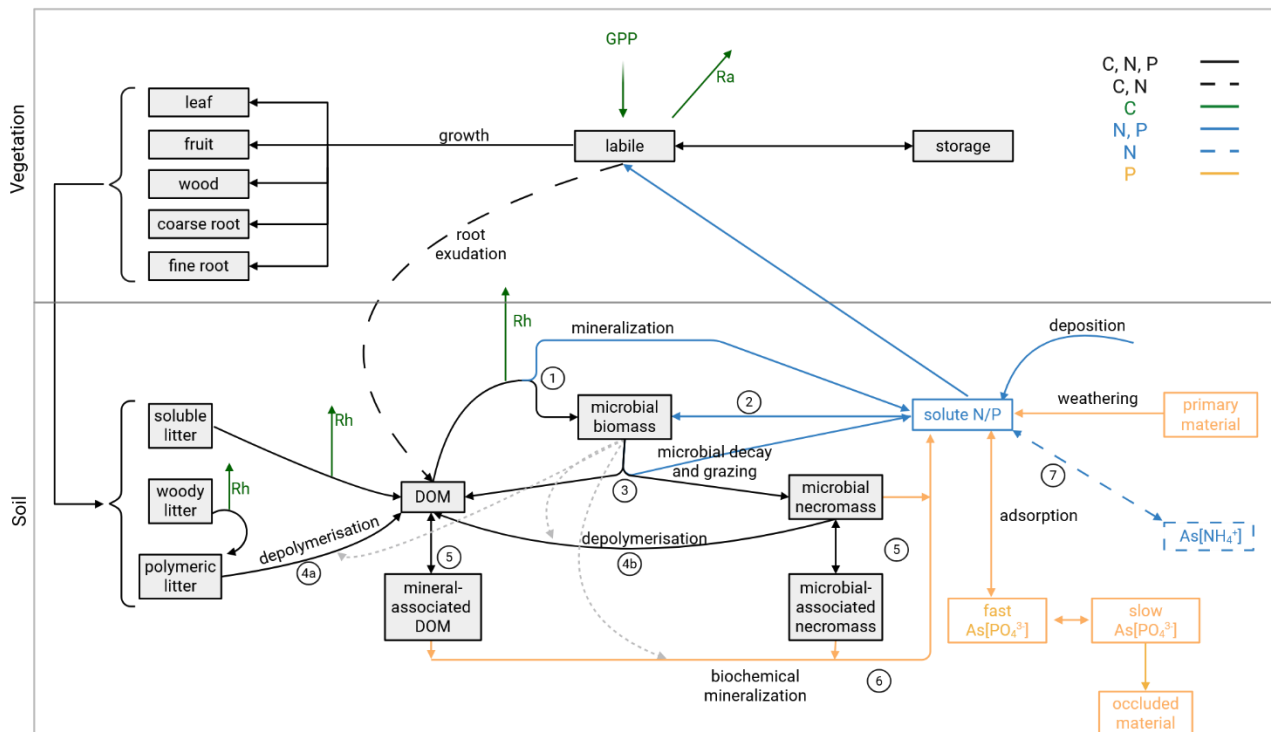
stoichiometry of target pools. Biochemical mineralization is assumed to be controlled by temperature, moisture, and the C: P stoichiometry of the target pools.

235 New N enters the system via deposition and asymbiotic N fixation (Fig. 2, process 7) and is lost by gaseous emission and lateral loss. New P enters the ~~systemssystem~~ via atmospheric deposition and weathering from parent material, which is controlled by abiotic and biotic factors. ~~On the other hand, PPhosphorus~~ is made irreversibly unavailable by occlusion or ~~leavesis lost from~~ the system by lateral loss.

240 **Table 1: Summary of soil pools in QUINCY-JSM, their turnover times and soil pools they represent.**

Pool in Quincy-JSM	Turnover time	Associated soil pools	Microbial availability
Soil organic matter (SOM)			
'free' DOM	emergent	DOM/POM	Direct available
Mineral associated dissolved organic matter	emergent	MAOM	Only available for biochemical mineralization (P only)
microbes	150 d	Microbial biomass	/
Microbial necromass	emergent	DOM/POM	Available for enzymatic decomposition
Mineral associated microbial necromass	emergent	MAOM	Only available for biochemical mineralization (P only)
Litter pools			
soluble	30 d	litter	Not directly available, turnover into DOM
polymeric	emergent	litter	Available via enzymatic decomposition
woody	2.5 yr	litter	Not directly available, turnover into polymeric litter





245 **Figure 2: Conceptual scheme of plant-soil interactions and soil processes in QUINCY-JSM.** Gross primary productivity determines carbon uptake by plants. Organic C, N₂ and P can enter the soil via litterfall and root exudation (C and N). Root litterfall and root exudation can enter deeper soil layers, while other litterfall is added to the topsoil layer. Boxes represent pools (clarified in Tab. 1) and solid arrows **represent** fluxes. All soil pools and fluxes are simulated for each soil layer. Soil pools of inorganic nutrients with **ASAs** [] represent mineral-associated pools (sorped to the soil mineral or organic surface). **Dashed Grey, dashed** arrows represent indirect **microbial influence on** processes **by microbes** via enzyme allocation. **RedBlack, solid** arrows represent fluxes of C, N and P. **Green, and black, dashed** arrows represent fluxes in C and N. **Green, solid arrows** represent C-only fluxes (**heterotrophic respiration, C uptake**). **Violet, Blue, solid** arrows represent N and P fluxes, **while blue, dashed arrows** refer to N-only fluxes. **Yellow, only arrows** refer to P fluxes; **blue, only N** fluxes. Modified from Yu et al. (2020). Created with BioRender.com

250

2.4 New implementation of dynamic root exudation in QUINCY-JSM

255 To improve the representation of soil-microbe interactions in QUINCY-JSM, we implemented a root exudation module (Fig. 3). Root exudation is modelled as direct, respiration-free flux from the plant labile pool to the soil DOM pool, with a C: N stoichiometry corresponding to the current C: N ratio of the plant labile pool (Fig. 2). As we assume that root exudation mainly consists of carbohydrates, amino acids and carboxylates (Jones et al., 2004), we do not model exudation of P. Implementation of root exudation thus reduces the C and N available for tissue growth and storage and thereby respiration despite no change

260 in the respiration calculations. From the DOM pool, the possible pathways for root exudates are: direct consumption by microbes, adsorption **towards to** the mineral surface or leaching.

The rate of root exudation [$\text{gC m}^{-2} \text{s}^{-1}$] is modelled as a function of fine root respiration [$\text{gC m}^{-2} \text{s}^{-1}$] and plant nutrient status (Eq. 1). We assume that physiologically active roots have increased exudation rate, and chose root respiration as **a** proxy for

tissue activity. Root respiration is simulated as a function of root N mass and root temperature. Observations support the positive relationship between root exudation and root respiration or root N content (Akatsuki and Makita, 2020; Li et al., 2021; Sun et al., 2017, 2021). Distribution of root respiration and exudation across the vertical soil profile follows the simulated root distribution. In addition, the slope of the linear relationship between root exudation and root respiration is assumed to be a function of nutrient status of the plant (Ataka et al., 2020; Prescott et al., 2020): C-to-nutrient ratios in the plant labile pool that are higher than the average C-to-nutrient ratios required for tissue production will result in higher exudation (Eq. 2).

$$CEX = s \cdot \beta_{mavg} \cdot R_{fr} \cdot \beta_{mavg} \cdot R_{fr} \quad (1)$$

Where CEX is C root exudation in $[gC\ m^{-2}\ s^{-1}]$, R_{fr} is fine root respiration in $[gC\ m^{-2}\ s^{-1}]$, s [unitless] is a unitless parameter that determines maximum slope and β_{mavg} [unitless] is the 7-~~days~~day moving average of a scalar β reflecting nutrient shortage and surplus C in the labile pool (range 0 - 1) (Thum et al., 2019), calculated by:

$$\beta = \frac{1 - e^{-(\lambda + \Phi)k_{ex}}}{1 - e^{-(\lambda + \Phi)k_{ex}}} \quad (2)$$

Where λ [unitless] and k_{ex} [unitless] are parameters (Table 2 for values used in this study) and the modifier Φ represents C excess, or N and P deficiency, respectively:

$$\Phi = \Phi_C \cdot \text{Max}(\Phi_N, \Phi_P, 1) \quad (3)$$

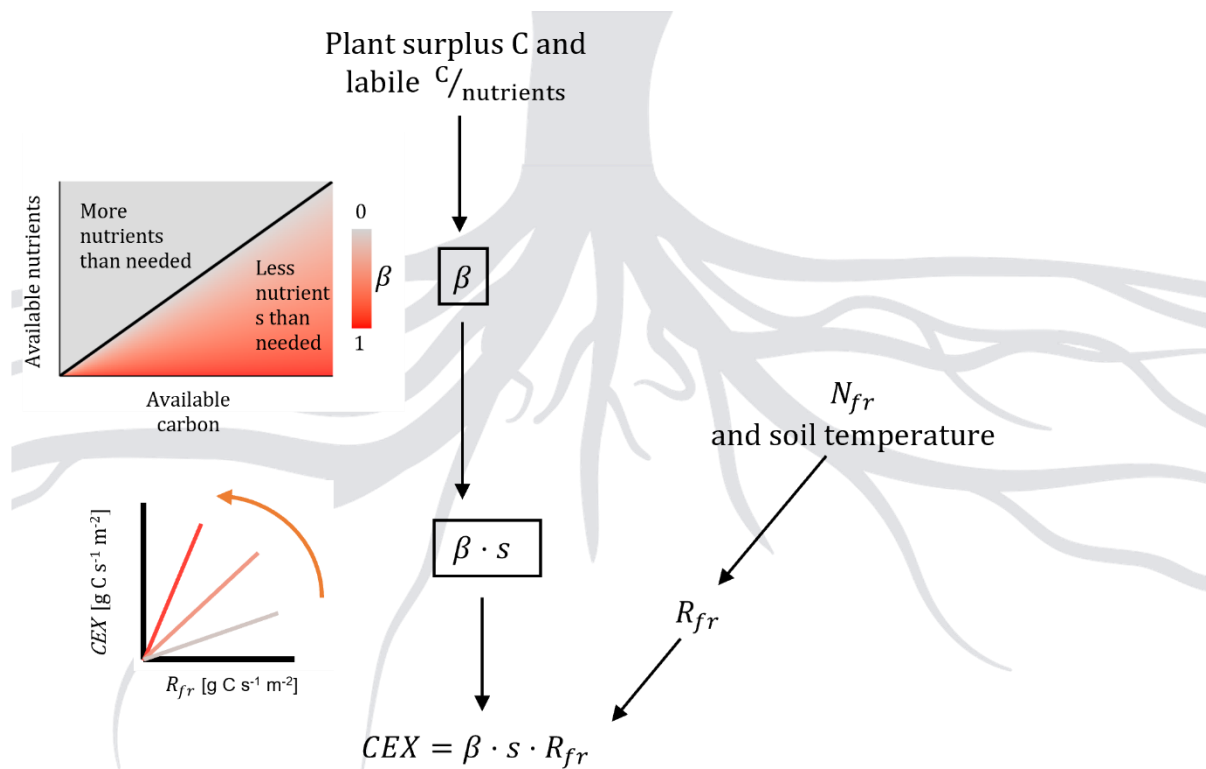
Where Φ_C is calculated as the ratio of the actual C-labile C pool size (C_{lab}) $[molC\ m^{-2}]$, compared to the target pool size (C_{lab}^*) $[gC\ m^{-2}]$. Φ_N and Φ_P are calculated as the ratio of labile pool stoichiometry ($(C/N)_{lab}$, $(C/P)_{lab}$ [unitless]) and labile pool target stoichiometry ($(C/N)_{lab}^*$, $(C/P)_{lab}^*$ [unitless]). The target labile C pool size (C_{lab}^*) is calculated as the maximum of either the weekly sum of GPP or maintenance respiration. The N and P target labile pool sizes are calculated based on the last 7-day stoichiometric ~~last 7 day~~ growth requirements in N and P to convert C_{lab}^* into plant biomass. The modifiers are given by:

$$\Phi_C = \text{MAX} \left(1, \frac{C_{lab}}{C_{lab}^*} \right) \quad (4)$$

$$\Phi_N = \frac{(C/N)_{lab}}{(C/N)_{lab}^*} \quad (5)$$

$$\Phi_P = \frac{(C/P)_{lab}}{(C/P)_{lab}^*} \quad (6)$$

As a result, Φ increases under conditions in which labile C accumulates in the labile pool, and if the stoichiometry of the labile pool is wider/higher than the target stoichiometry. The smallest value that Φ can take is 1, leading to values of β close to zero. We constrained β to values larger than 0.0125 (β_{min}) ~~reflecting~~, to ensure a minimal root exudation flux equal to 5% of fine root respiration, even at nutrient-saturated conditions.



320 | **Figure 3: Conceptual model of the nutrient modifier for carbon root exudation (CEX). Detailed description in Eq. (1–6). CEX is calculated proportional to fine root respiration (R_{fr}). Higher C surplus or higher C-to-nutrient ratio than needed for growth leads to increase in the modifiers. This is translated into a steeper slope for the relationship between root exudation rate and fine root respiration. Fine root respiration is calculated by fine root N content (N_{fr}), accounting for the influence of temperature on maintenance respiration. Created with BioRender.com**

Table 2: dynamic root exudation parameters

Parameter	Description	Value used for this simulation	reference
s	Slope conversion factor/ maximum slope	4	This study
β_{min}	Minimal value for β	0.0125	This study
k_{ex}	Weibull parameter for beta	2	Thum et al., 2019; following sink limitation
λ	Weibull parameter for beta	0.05	This study; following sink limitation

325 2.5 EucFACE experimental site and measurement data

The EucFACE site is located in Western Sydney, Australia (33° 37' S, 150° 44' E, 30 m in elevation) in a mature eucalypt woodland. For a detailed description of the site see (Drake et al., (2016;) and Ellsworth et al., (2017). The site has a subtropical transitional climate with an annual average temperature of 17 °C and mean precipitation of 800 mm yr⁻¹. Overstorey vegetation is dominated by *Eucalyptus tereticornis*, while understorey vegetation consists of a diverse mixture of shrubs, 330 graminoids, and forbs dominated by *Microlaena stipoides* (Piñeiro et al., 2020).

The soil is characterized as ~~aeric podosol~~ Aeric Podosol with a loamy sand texture up to 50 cm and a sandy clay loam texture in deeper horizons. The soil has a slightly acidic pH and low fertility (Crous et al., 2015; Ross et al., 2020). Previous experiments showed that plant growth is P-limited (Crous et al., 2015). Available soil P; and plant P to soil P ratio are similar to tropical and subtropical ecosystems (Jiang et al., 2024b).

335 The EucFACE experiment consists of 6 FACE rings, with a 25 m diameter. Three rings received aCO₂ levels and three rings were exposed to eCO₂ levels (ambient +150 ppm). In 2012, CO₂ was stepwise increased over a period of six months with an increase of 30 ppm every 5 weeks. In February 2013, the CO₂ concentration in the experiment rings reached their target of +150 ppm (Drake et al., 2016). Since then, the ecosystem has been continuously exposed to eCO₂. Measurements used in this study were taken between 2013—2019. Major C pools, ~~net primary biomass~~ production (NPPBP) and net ecosystem 340 production (NEP) under ambient conditions were measured between 2013—2016. A detailed description ~~of~~ measurement methods is provided in (Jiang et al., (2020) and (Jiang et al., (2024b). Soil respiration is taken from (Drake et al., (2018) and supplemented by additional information from (Jiang et al., (2020).

2.6 Model parameterization

We parameterized the model following in situ-based observations for *E. tereticornis*, taken under ambient conditions from 345 2013—2019, provided by (Jiang et al., (2024a) (Table A1). As no direct measurements of root exudation exist for this site, we calibrated s and β_{min} to reproduce GPP, biomass and soil respiration for ambient conditions from 2013—2016 (Jiang et al., 2020) (Table B1). ~~By this we limit~~ This limits the size of the root exudation flux. We ensured that the modelled exudation flux still responded to variations in the size and stoichiometry of the labile plant pool, ~~i.e., meaning~~ that the flux was not controlled by empirical bounds of maximum exudation, implying that it is sensitive to changes in plant carbon and nutrient 350 status induced by eCO₂.

2.7 Model set-up and analysis

Simulations were done for 500 years of spin-up to reach quasi-equilibrium, with a subsequent simulation length of 325 years afterward from 1700—2024, following the modelling protocol from (Jiang et al., (2024a): Meteorological forcing for 1700—2012 and 2019—2024 was gained from repeated and randomized observations from 2013—2018, while CO₂, N_x and P 355 deposition followed historic values. Forcing for spin-up repeated the first 30 years of the forcing data under 280 ppm CO₂. As

a result of forcing from randomized observations and meteorological extremes in observation years, and contrary to observations, our model showed a downward trend in total vegetation C from 5900 gC m⁻² to 5700 gC m⁻² between the years 2012 and 2019 (Fig. B1). The trend did not cause major pulses in nutrient input and therefore unlikely reflects in CO₂ affects eCO₂ effects on nutrient-dependent root exudation and microbial C cycling.

360 The mean yearly change in pools and mean yearly fluxes for simulations were calculated for 2013–2019. We calculated the effect of eCO₂ by subtracting results under aCO₂ conditions from results under eCO₂. We compared the results to observed effects of eCO₂ on the C budget described in (Jiang et al., (2020).

We trace the fate of the additionally assimilated C under eCO₂, through the ecosystem. We standardize fluxes as the percentage of additional overstorey GPP for both simulations and observations. The model currently only simulates forests without
365 understorey vegetation. To maintain comparability, we use observations from overstorey aboveground biomass production, overstorey autotrophic respiration, and overstorey changes in vegetation C pools. However, for belowground fluxes, i.e., heterotrophic respiration, root respiration, root biomass production and changes in soil C pools, we cannot differentiate between overstorey and understorey origin. We still standardize them as the percentage of additional overstorey GPP but are therefore likely to overestimate the observed change per additional overstorey GPP under eCO₂ in soil fluxes.

370 For model analysis, microbial growth was calculated by the flux from the DOM to the microbes ($F_{DOM \rightarrow MIC}^X$ [gX m⁻² s⁻¹]), adjusted by the current carbon-use or nutrient-use efficiency (XUE [unitless]) for each soil layer separately. Most measurements for soil processes at EucFACE were taken in topsoil layers, which are also typically more active. We therefore separate model outputs between topsoil (upper 50 cm) and deep soil (below 50 cm). We estimate the contribution of fluxes
375 from root exudation, microbial recycling upon death, and decomposition of soluble litter, polymeric litter, and microbial necromass to microbial growth $F_{i \rightarrow growth}^X$ [gX m⁻² s⁻¹] for topsoil by based on their relative production of DOM:

$$F_{i \rightarrow growth}^X = F_{DOM \rightarrow MIC}^X * XUE * \frac{F_{i \rightarrow DOM}^X}{\sum_{i \in I} F_{i \rightarrow DOM}^X} \cdot \frac{F_{i \rightarrow DOM}^X}{\sum_{i \in I} F_{i \rightarrow DOM}^X} \quad (6)$$

With I being the set of all contributing pools and $F_{i \rightarrow DOM}^X$ [gX m⁻² s⁻¹] being the according contributing fluxes from these pools towards to DOM. Similarly, we calculated heterotrophic respiration derived from the depolymerization of necromass C,
380 $Rh_{priming}$ [gC m⁻² s⁻¹] as follows:

$$Rh_{priming} = F_{DOM \rightarrow MIC}^C * (1 - CUE) * \frac{F_{necromass \rightarrow DOM}^X}{\sum_{i \in I} F_{i \rightarrow DOM}^C} \cdot (1 - CUE) \cdot \frac{F_{necromass \rightarrow DOM}^X}{\sum_{i \in I} F_{i \rightarrow DOM}^C} \quad (7)$$

2.7.1 Turnover times

To account for adaptation to sudden CO₂ increase, turnover times were calculated for 2015-2019. Soil turnover times τ_{soil}^X [yr] were calculated by dividing pool sizes with by their respective outgoing fluxes as follows:

385

$$\tau_{soil}^C = \frac{C_{litter} + C_{soil}}{R_h} \quad (8)$$

$$\tau_{soil}^N = \frac{N_{litter} + N_{soil} + N_{inorg}}{leaching_N + U_N^{plant} + emission_N} \quad (9)$$

$$\tau_{soil}^P = \frac{P_{litter} + P_{soil} + P_{inorg}}{leaching_P + U_P^{plant} + occlusion} \quad (10)$$

Where X_{litter} are the combined litter pools; X_{soil} are the combined organic topsoil pools and X_{inorg} as combined inorganic topsoil pools [$gX\ m^{-2}$]. ~~In the denominator are processes~~ Processes removing N or P from topsoils, e.g., heterotrophic respiration

390 R_h , leaching, occlusion, emission and plant uptake U_X^{plant} [$gX\ m^{-2}\ yr^{-1}$], are in the denominator.

~~necromass~~ Necromass turnover $\tau_{necromass}^X$ [yr] time was calculated as

$$\tau_{necromass}^C = \frac{C_{necromass}}{F_{residue \rightarrow DOM}^C} \quad (11)$$

$$\tau_{necromass}^N = \frac{N_{necromass}}{F_{residue \rightarrow DOM}^N} \quad (12)$$

$$\tau_{necromass}^P = \frac{P_{necromass}}{F_{residue \rightarrow DOM}^P + Biochem_{minnecro}} \quad (13)$$

395 Where $X_{necromass}$ [$gX\ m^{-2}$] is the combined pool of microbial necromass and mineral-associated microbial necromass and $Biochem_{minnecro}$ [$gP\ m^{-2}\ yr^{-1}$] is the biochemical mineralization from these pools.

3 Results

3.1 Model evaluation

400 3.1.1 Model performance under ambient conditions

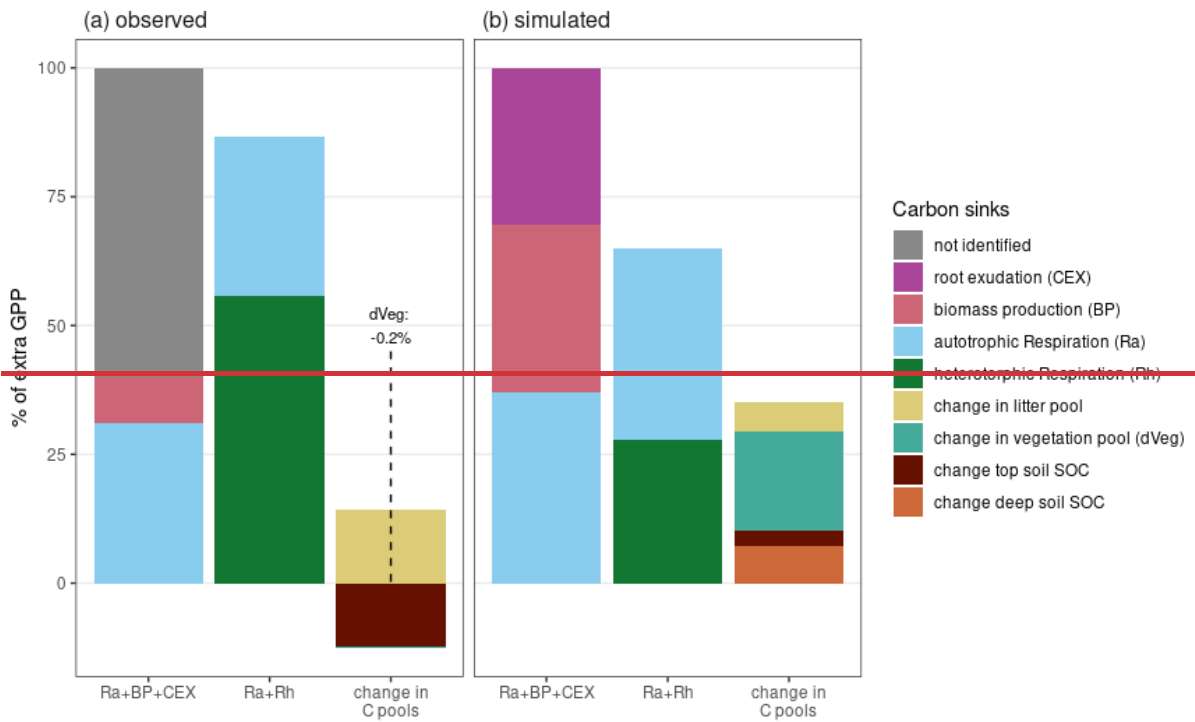
Simulated vegetation and soil ~~pools-size~~pool sizes and stoichiometry, and ecosystem fluxes under ambient conditions are in the range of observations from the three control plots for the period of 2013—2016 (Table B1, B2). Simulated GPP had a 9 % bias, but was still within one standard deviation of the observation-based estimate. However, the model underestimated BP by 25-%. Modelled soil respiration under ambient conditions was around $1207 \text{ gC m}^{-2} \text{ yr}^{-1}$, and thus slightly larger than the
405 observed range of $1097 (\pm 86) \text{ gC m}^{-2} \text{ yr}^{-1}$. The model estimated that soil respiration was 61% heterotrophic and 39% autotrophic root respiration, which agree/agrees well with observations that estimated 56% and 44%, respectively (Jiang et al., 2020). There are no direct observations of root exudation at EucFACE, but the model estimated mean C root exudation (CEX) to be $366 \text{ gC m}^{-2} \text{ yr}^{-1}$ for ambient conditions, equivalent to 22% of GPP. Exudation rate per gC fine root biomass amounted to $2 \text{ gC (gC fr)}^{-1} \text{ yr}^{-1}$ and ranged from $0.1 \text{ mgC (gC fr)}^{-1} \text{ d}^{-1}$ to $16 \text{ mgC (gC fr)}^{-1} \text{ d}^{-1}$ on a daily level, with an average
410 C to N ratio of 176 gC gN^{-1} .

3.1.2 Allocation patterns of additionally acquired GPP

Our model simulated an increase in GPP and root exudation under eCO₂ (Table B3). Elevated CO₂ increased simulated annual GPP (2013—2019) by 22%. Simulated annual root exudation and BP increased 30% and 33% respectively and therefore increased stronger/more than GPP (Fig. B2). While our simulations indicate, as suggested by observations, an increase in
415 belowground allocation through root exudation, the model overestimated the observed effect in GPP (12%) and biomass production (3%). Soil respiration increased by 13%, agreeing with the observed 12% increase, although remaining lower than the 22% GPP increase. Overall, eCO₂ caused only minor shifts in plant C allocation (Fig. B2).

We further traced the fate of additional GPP and compared it with the findings from Jiang et al. (2020) to see if our implementation improves plant C allocation under eCO₂ (Fig. 4, detailed numbers in the supplement; Fig. B3). Our model
420 estimated that vegetation allocated 30% of additional GPP under eCO₂ to root exudates, providing a possible explanation for the unidentified flux in observations (Fig. 4, $Ra+BP+CEX$). Since in ~~our~~the model eCO₂ increased BP, the model allocated, contrary to observations, 33% of additional GPP to BP, and increased vegetation pools under eCO₂ (Fig. 4, $Ra+BP+CEX$, *change in C pools*). Our model simulated that 28% (Fig. 4b, $Ra+Rh$), lower than the observed 56%, of additional GPP was respired as soil heterotrophic respiration (Rh). This difference may result from underestimation of the effect of eCO₂ ~~in~~on root
425 exudation and overestimation of allocation to BP, but may also be caused by normalizing the observed soil respiration response with GPP response derived solely from the overstory. Observations indicated a decrease of topsoil organic C equal to -12% of the change in GPP under eCO₂ during the experimental phase, but the result was not significant. In our simulation, eCO₂ led to an increase of topsoil C equal to 3% of the change in GPP. However, the model also simulates an accumulation of C in deeper soil layers equal to 7% of the additional C uptake, likely caused by increased root exudation in deeper soil layers.

430 Considering the strong variation in measurements regarding soil organic C (SOC) pools, we assume that our simulations are in agreement with observations regarding topsoil C pools. Overall, our model supports the previous hypothesis from observations that a large portion of additional GPP was allocated to root exudation but caused only minor increases in SOC in topsoils (Jiang et al., 2020, 2024a).



435

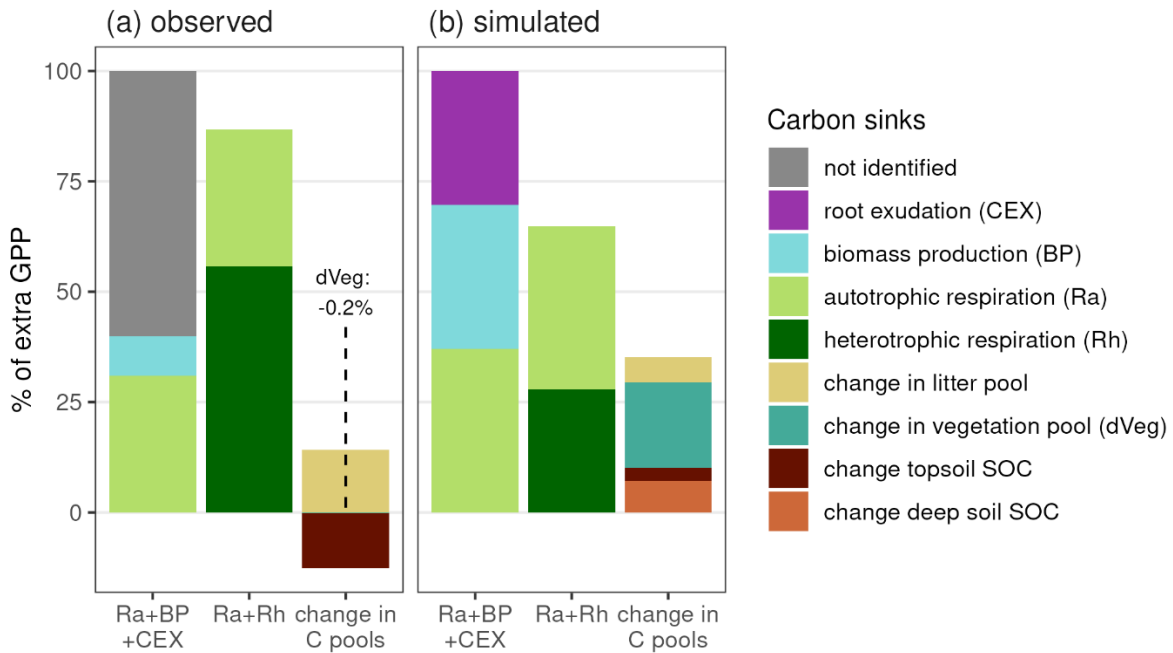


Figure 4: Comparison of the fate of additional sequestered C under $e\text{CO}_2$ as percentage of increased overstorey gross primary productivity (GPP) for a) observations (2013–2016) (Jiang et al., 2020) and b) simulations (2013–2019). For simulations additional GPP is transferred into autotrophic respiration (Ra), biomass production (BP), and root exudation (CEX). For observations CEX was not measured. Ecosystem respiration is composed of autotrophic respiration (Ra) and heterotrophic respiration (Rh). Changes in ecosystem C pools is C pools are composed of changes in topsoil organic C (10 cm for observation, top 50 cm for simulation), changes in deep soil SOC (no observations), changes in litter pool and changes in vegetation (dVeg).

3.2 Simulated effects of $e\text{CO}_2$ on microbial processes

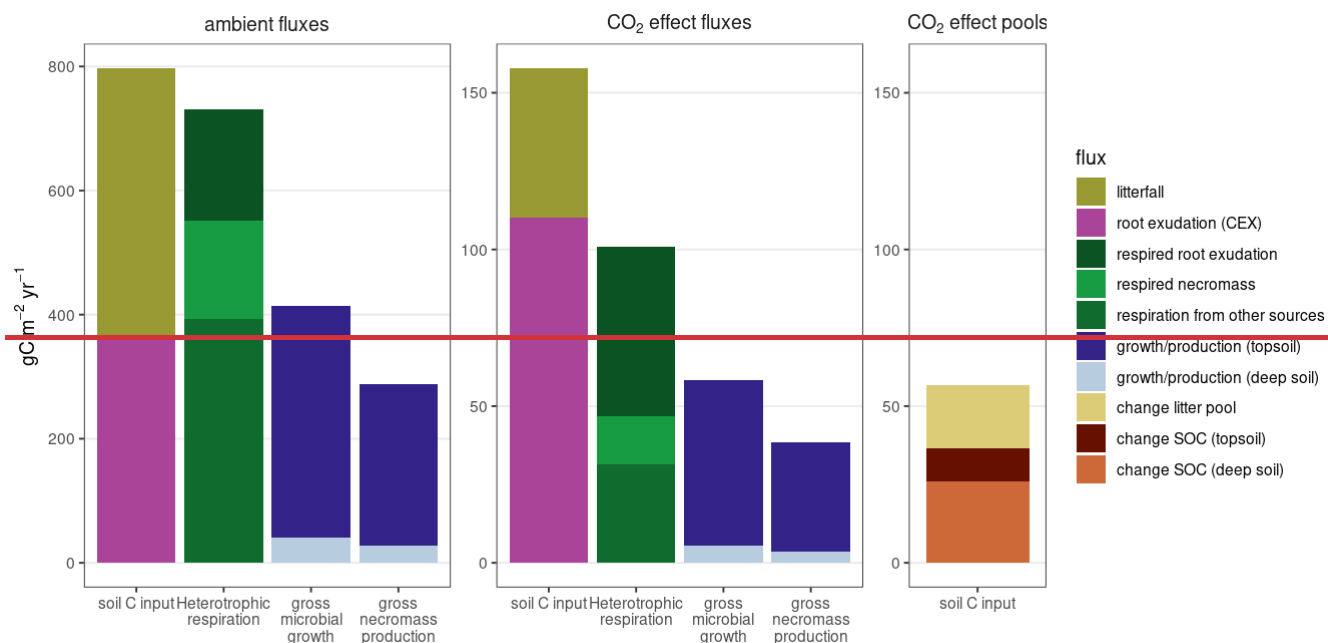
3.2.1 Microbial growth and respiration

In the model, $e\text{CO}_2$ increased belowground input disproportionately through high root exudation, increasing heterotrophic respiration and microbial growth (Fig. 5, detailed numbers in the supplement). Our model suggests that under ambient conditions, 45% of C flux into soils originated from root exudation. Heterotrophic respiration under $a\text{CO}_2$ matched 92% of the input to 92%. The majority of heterotrophic respiration (54%) originated from decomposition of litter and microbial recycling upon turnover. Microbial growth occurred mostly in topsoil layers. In the simulation, $e\text{CO}_2$ increased both biomass production and root exudation, resulting in a 20% increase ($158 \text{ gC m}^{-2} \text{ yr}^{-1}$) in soil C input compared to ambient conditions. This additional C input under $e\text{CO}_2$ was composed of 70% root exudation and 30% litter (Fig. 5, soil C input). The additional heterotrophic respiration (Fig. 5, Heterotrophic respiration) was 50% driven to 50% by respiration of fresh root exudation, suggesting that root exudates in topsoil layers are directly consumed by microbes, and then respired according to the assumptions for CUE. In the model, CUE for microbial growth is dependent on the stoichiometric imbalance between

455 the source material and microbial biomass, and constrained within a range of 30% to 50%. ~~Further~~ ~~A further~~ 15% of additional heterotrophic respiration under eCO₂ ~~were~~~~was~~ caused by decomposition of necromass, i.e., priming.

In ~~our~~~~the~~ model, gross microbial growth and necromass production increased by 14% and 13%, respectively, compared to ambient conditions (Fig. 5, *microbial and necromass growth*). This means that only 34% of the additional C input resulted in gross microbial growth in topsoils and only 22% of the additional C input resulted in gross necromass production in topsoils.

460 Simulated net topsoil SOC increase was small compared to overall additional C input (10 gC m⁻² yr⁻¹, 6% of the additional C input) (Fig. 5, *change in C pools*). Increased respiration of necromass, i.e., ~~...~~ priming, suggests that additional gross necromass production was offset by microbial nutrient acquisition.



465

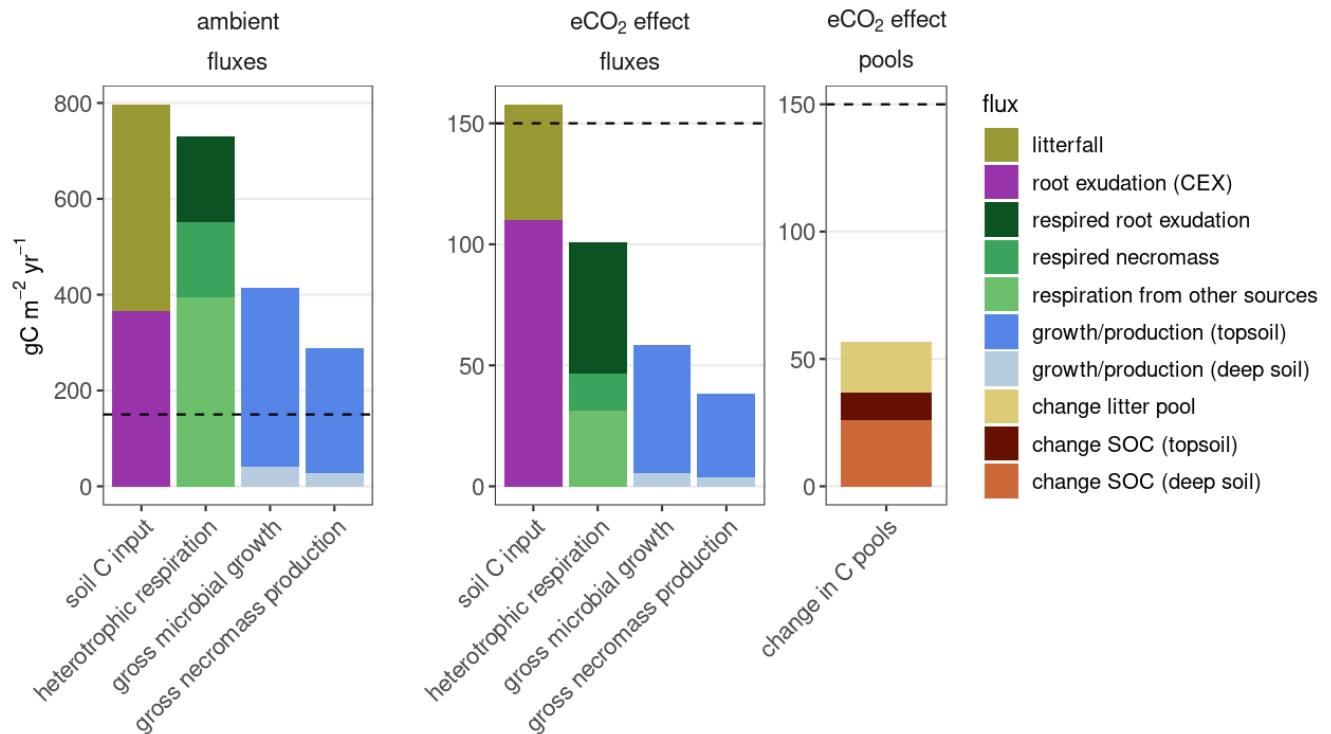


Figure 5: ~~simulated~~ Simulated sources and sinks for C in soil at EucFACE under ambient conditions and as ~~eCO₂~~ the eCO₂ effect, displayed as yearly average for 2013–2019. Additional C input is composed of litterfall and exudation (CEX). Elevated CO₂ induced increased heterotrophic respiration (Rh), which originated from respiration of exudation, respiration of microbial necromass, and respiration of other sources, like degradation of woody biomass and respiration of directly recycled microbial biomass, soluble and polymeric litter. Additionally, eCO₂ affects growth-increased gross microbial C-growth and gross necromass production topsoil and deep soil, change in litterpools, Elevated CO₂ increased litter pool, topsoil (50 cm) soil organic carbon (SOC) and deep soil SOC.

3.2.2 Microbial resource acquisition

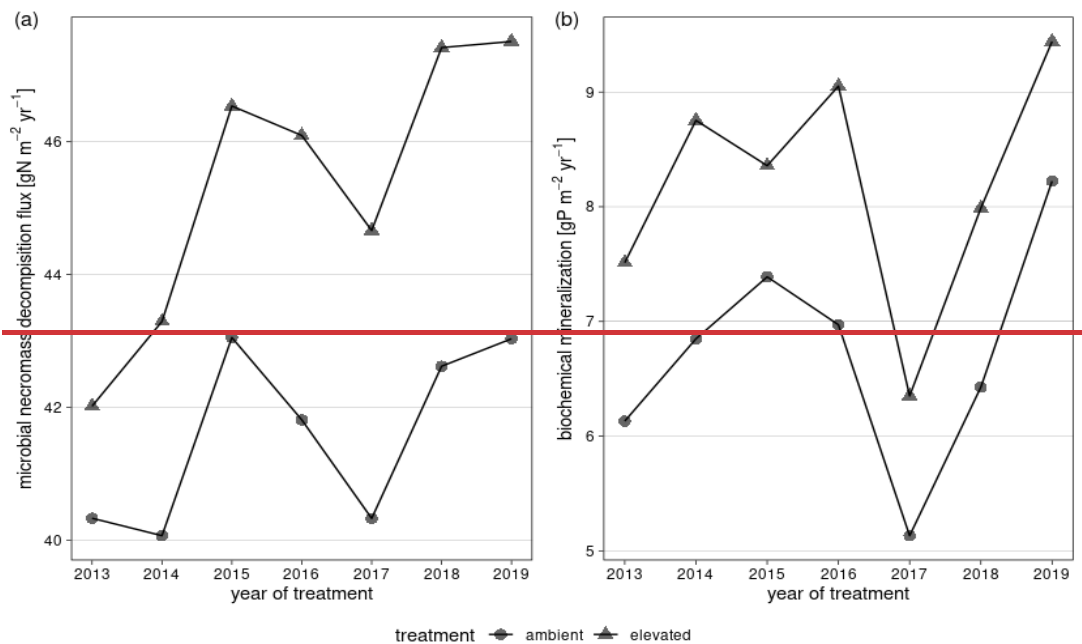
In the model, increased gross microbial growth led to higher absolute microbial nutrient uptake from organic sources (Fig. 6).

Absolute decomposition of microbial necromass increased by 9-% compared to ambient conditions, and mean annual biochemical mineralization increased by 22-% (Fig. 6, detailed numbers in the supplement). As a consequence, eCO₂ resulted in a 40-% increase in annual net PO₄ mineralization (Fig. B4).

Despite causing higher nutrient demands, eCO₂ did not cause a substantial shift in the relative contribution of nutrient sources to gross microbial growth for N and P (Fig. 7, detailed numbers in the supplement). For C, the contribution of root exudation increased from 30% to 34-% (Fig. 7-a7a). However, root exudates contributed only minimally to microbial N uptake and not at all to microbial P uptake, as the model assumes a high C:N ratio and no P in root exudates (Fig. 7 b, e7c). Microbial N was derived to 77-% (eCO₂: 75-%) from organic sources such as microbial recycling and depolymerized microbial necromass (Fig.

7-b7b). For P, 45% (eCO₂: 46%) of microbial P acquisition came from uptake of soluble phosphate (Fig. 7 c), most of which was solubilized via biochemical mineralization (Fig. B5).

485 Changes in nutrient source contributions were limited by model assumptions and the simulated nutrient conditions. Recycling of microbial biomass ~~upon~~ turnover is controlled by a constant; therefore, we expect little change regarding this flux. For N, NH₄ availability and flexibility in asymbiotic N fixation were sufficient to meet inorganic N demand, preventing an increased reliance on decomposition. Microbial P uptake through decomposition of microbial necromass was controlled by microbial C and N limitation.



490

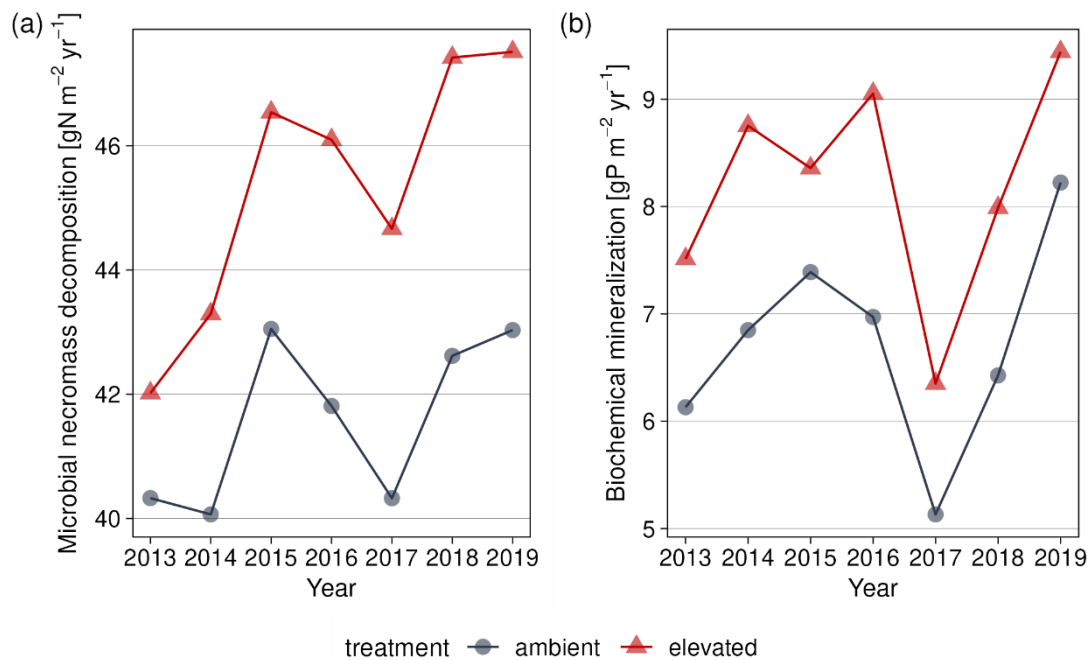
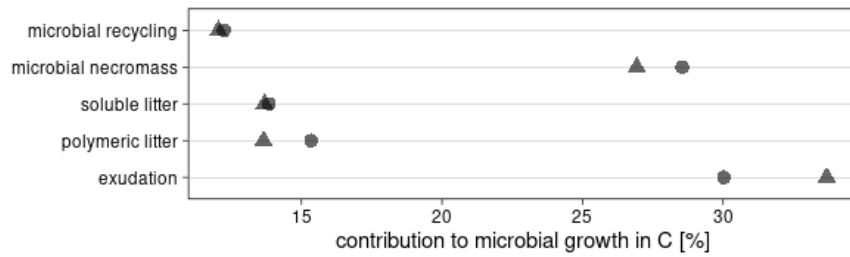


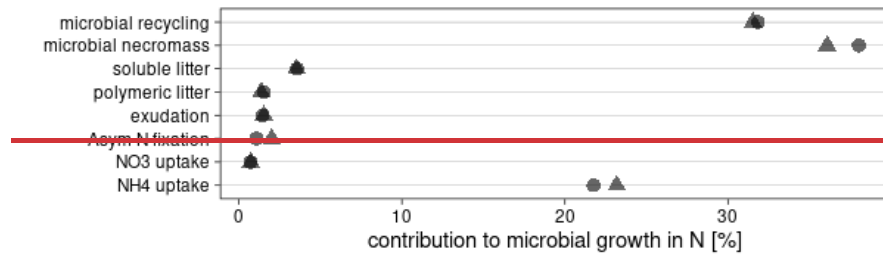
Figure 6: Simulated annual mean of main fluxes for microbial, enzyme-mediated nutrient acquisition from organic matter for topsoil in treatment years for 2013–2019. a) Annual microbial necromass decomposition for N acquisition. b) Biochemical mineralization from necromass, mineral-associated microbial necromass, and mineral-associated DOM.

495

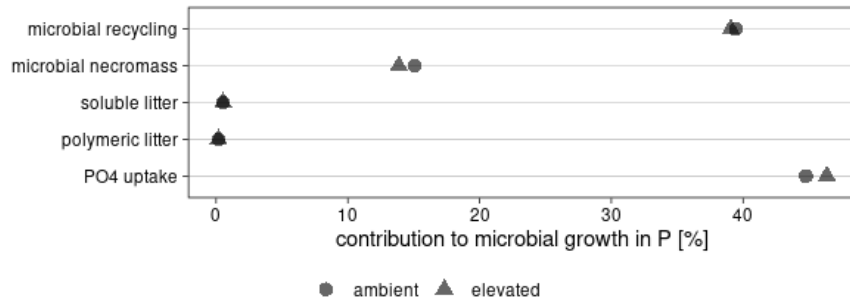
(a)

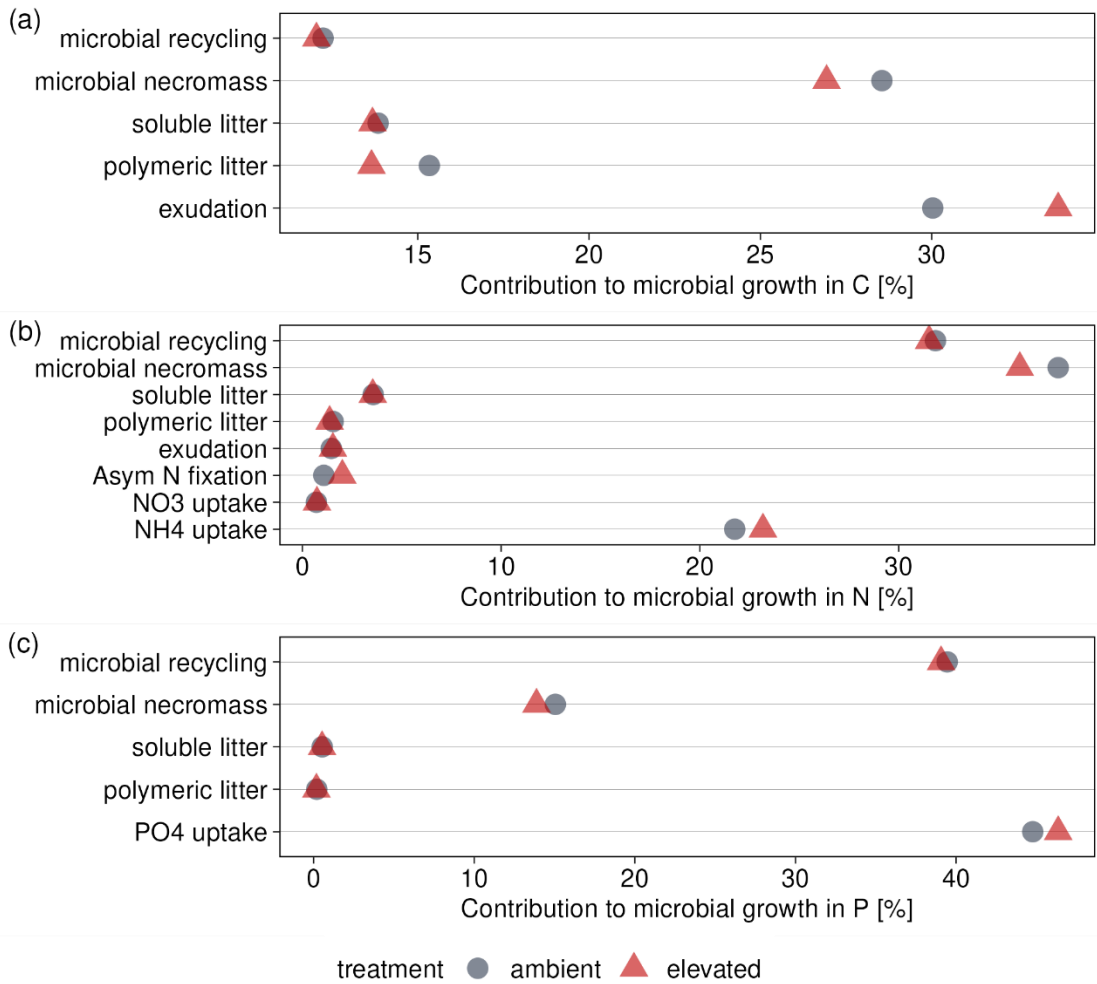


(b)



(c)





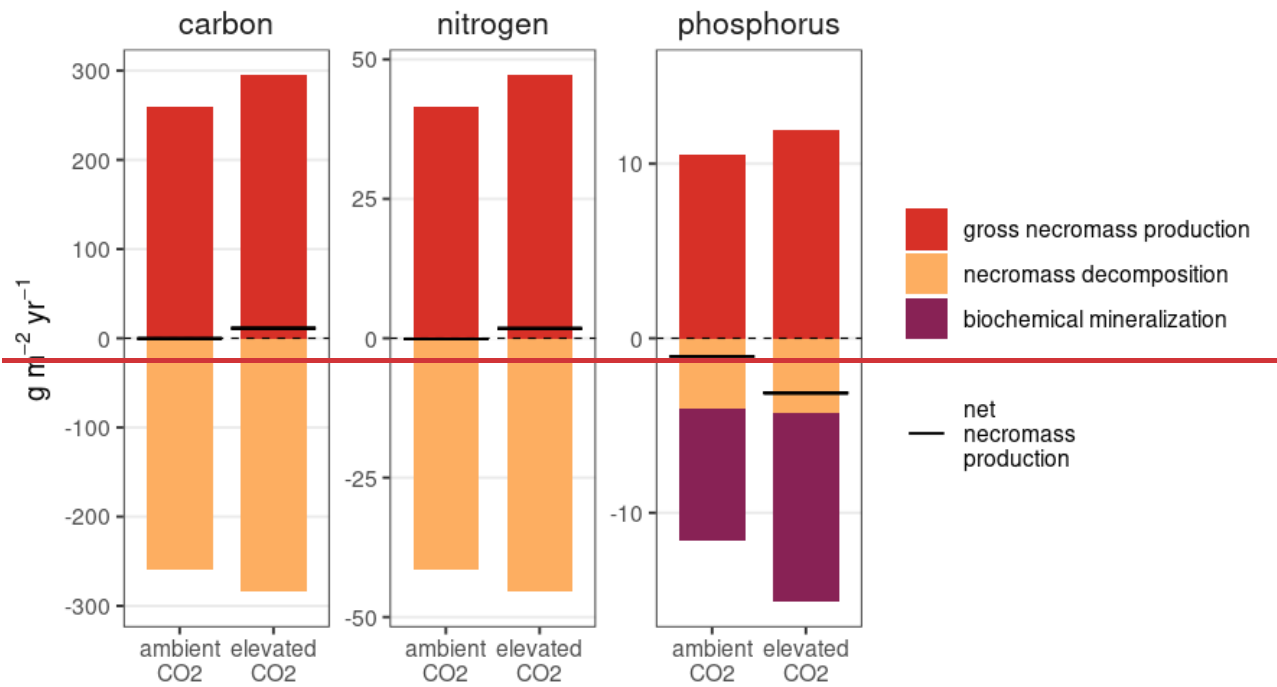
500 **Figure 7: Simulated distribution of nutrient sources for gross microbial growth under ambient and elevated conditions for gross microbial growth at EucFACE in topsoil (50 cm) averaged for 2013–2019, for a) carbon, b) nitrogen, c) phosphorus. Contributions were calculated based on the contribution of sources to DOM and microbial CUE. Sources of gross growth are given for a) carbon, b) nitrogen, c) phosphorus, use efficiency. For P, a significant substantial amount of PO₄ is gained by biochemical mineralization of organic material (Fig B-rev-2B5).**

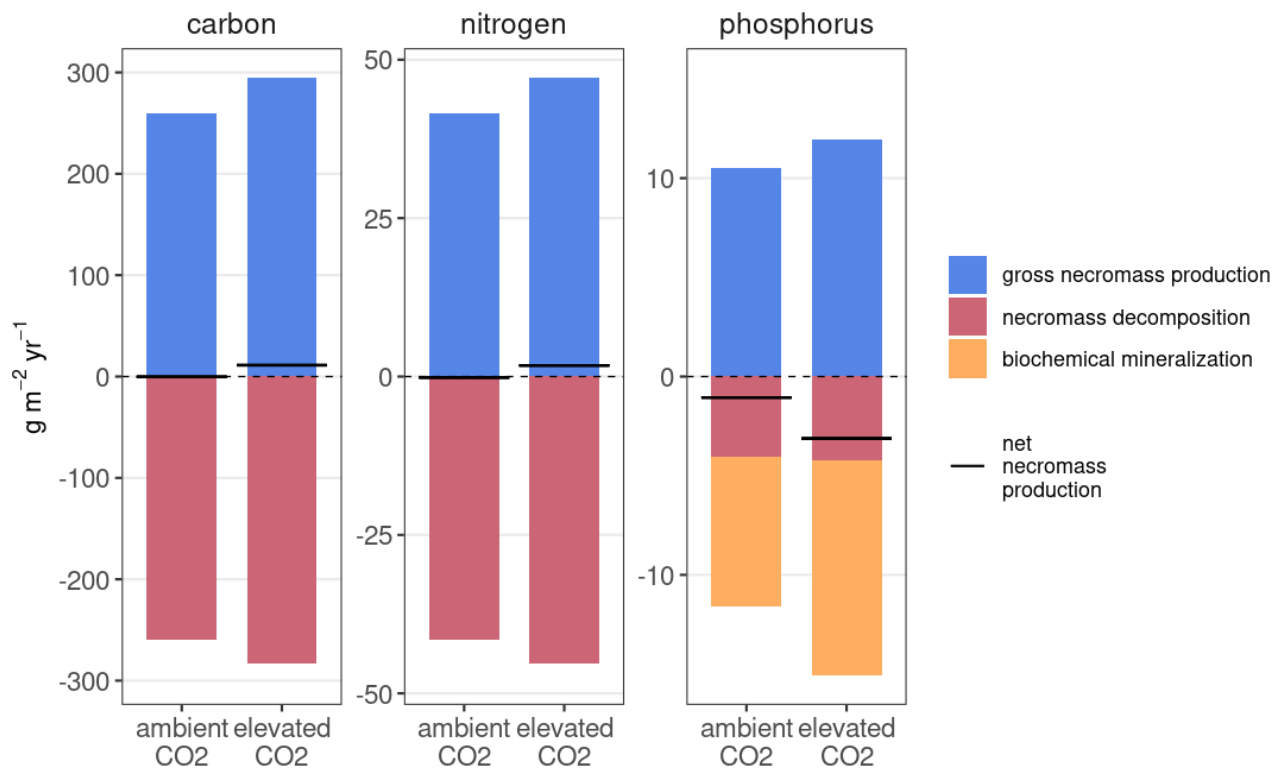
3.2.3 Net necromass production

505 We summarized simulated gross production, decomposition and biochemical mineralization of microbial necromass (“free” necromass and mineral-associated necromass) in the topsoil (Fig. 8, detailed numbers in the supplement). Increased in- and outgoing fluxes to microbial necromass accelerated turnover of SOM (Tab. B-4 Table B4). Elevated CO₂ increased gross necromass production for C, N₂ and P by 13% (Fig. 8). However, increased depolymerization and biochemical mineralization under eCO₂ also increased outgoing fluxes (in C: (9-%,%), N: (9-%,%), and P: (30-%)). Regardless of treatment, net effects in cycling of microbial-C necromass were small for all elements relative to the size of in- and outgoing fluxes and pool sizes.

520 Under aCO₂, net necromass production in C and N was close to zero, whereas under eCO₂, net production was positive, causing a 12 gC m⁻² yr⁻¹ and 2 gN m⁻² yr⁻¹ necromass increase compared to ambient conditions. Net necromass production of P was -1 gP m⁻² yr⁻¹ under aCO₂ and -3 gP m⁻² yr⁻¹ under eCO₂. However, eCO₂ decreased the overall necromass P pool only 2% (-2 gP m⁻² yr⁻¹). Phosphorus remained in the ecosystem and was transferred to faster cycling pools, namely microbial biomass or dissolved organic matter (Fig. B6, Fig. B7).

525 As, in the model, C and N cycling of microbial necromass are closely interlinked, turnover times of microbial necromass decreased by 9% for C and N (Table B4). For P, enhanced biochemical mineralization further decreased necromass turnover time by 21%. Combining all soil pools, elevated CO₂ had a more pronounced effect on P (20% decrease) and N (20% decrease), then on C cycling (12% decrease), possibly caused by increased inorganic nutrient cycling.





530 **Figure 8: Simulated balance of C, N and P for microbial necromass (combined pool of microbial necromass and mineral-associated microbial necromass) in topsoil (50 cm) under ambient and elevated CO₂. Gross production (red/blue, above the dashed line) are compared with decomposition (yellow/red, below the dashed line) and, for P, biochemical mineralization (purple/yellow, below the dashed line). Black lines represent the net necromass production.**

4. Discussion

535 We developed and tested a model implementation for dynamic root exudation in a microbial-explicit terrestrial biosphere
model and analyzed the consequences for increased root exudation under eCO₂ in a mature Eucalyptus forest. We found that
– in ~~our~~the model – increased root exudation links enhanced GPP and heterotrophic respiration under eCO₂ and improved
simulated allocation of additional GPP (~~Fig. to ecosystem fluxes, compared to simulations without root exudation~~ (Fig. 4, Fig.
B8, Fig. B9). Increased root exudation caused only minor increases in topsoil C, as more than 60-% of additional C input into
540 soils was matched with~~by~~ increased heterotrophic respiration and eCO₂. This was primarily caused by soil microbes respiring
a substantial amount of the new C input, with an additional contribution through enhanced necromass decomposition for
microbial N acquisition. Microbial P demands were primarily met by biochemical mineralization. Simulated results are
constrained by model uncertainties and assumptions.

4.1 Plant carbon allocation and root exudation

545 Our simulations indicate that increased root exudation is a major pathway for belowground C allocation under eCO₂, but the
magnitude is difficult to validate due to the absence of direct measurements at EucFACE. Our model estimated a root
exudation-to-GPP ratio of 21-% under ambient conditions, which is substantially higher than global estimates (Chari et al.
2024). Chari et al. (2024) ~~suggests~~suggest a global mean of 5.6-% based on upscaling measurements of free root exudation,
primarily taken with the cuvette method (Phillips et al., 2008). Due to the lack of such measurements at EucFACE, we estimate
550 root exudation from the ambient C budget. Our estimate therefore also includes other belowground allocations, e.g.,
mycorrhiza and losses through mucilage, and root exudation in deeper soil layers, which likely explains the differences between
our results and global estimations (Brunn et al., 2025; Johansson et al., 2009; Jones et al., 2004).

Simulated C allocation to root exudation increased by 30-% under a 22-% increase in GPP under eCO₂, consistent with the
observation-based hypothesis of increased belowground C allocation at EucFACE. Elevated CO₂ also enhanced mean annual
555 root exudation rate per unit fine root mass by 18-% (Fig. B2). Our estimates are lower than increases reported at other FACE
experiments. In Duke FACE allocation to exudates and fungi, increased by 40-% in upscaled annual flux per unit land area
(Drake et al., 2011). At BIFoR FACE, specific C exudation (~~ug/ug~~ g fine root ~~/dayd⁻¹~~) increased by 41–135% (P=0.037)
(Reay et al., 2025), and upscaled annual flux per unit land area by 43–63% (P = 0.042) (Norby et al., 2024).

Uncertainties in exudation rates at EucFACE remain considerable. We parameterized our model using ambient GPP and plant
560 pool observations and calculated root exudation flux ~~base~~based on fine root N concentration. The deviation from simulated
BP and fine root C:N ~~to~~from observations ~~leads~~lead to parameter uncertainty. The compiled C budget suggests increased C
allocation belowground under eCO₂ (Jiang et al., 2020), but a direct evaluation of ~~the~~-root exudation is not possible, also due
to large uncertainties associated with other components of the C budget. Additionally, our model only simulates the response
in overstorey vegetation, whereas the understorey vegetation at EucFACE showed a strong ~~NPP~~BP increase that likely affected

565 soil processes (Jiang et al., 2020; Piñeiro et al., 2023). Overall, more empirical data on belowground C allocation would aid the development and evaluation of TBMs.

The model also simulated a 33-% increase in overstorey BP under eCO₂, which was not observed in EucFACE. In the simulation, C accumulated primarily in woody biomass and the labile plant pool (Fig. B10), but this had only a minor influence on soil processes because plant litter contributed little to microbial growth in C, N₂ and P in the treatment period (Fig. 7).
570 Instead, root exudation dominated the additional C input and the supply to microbial growth under eCO₂. Observational studies suggest that plant P limitation suppressed plant growth under eCO₂ (Jiang et al., 2020), suggesting that the model likely underestimates P constraints or overestimates plant adaptability to P limitation.

Despite these limitations, our model closes the gap between increased GPP and observed increased heterotrophic respiration under eCO₂, underlining the importance of root exudation as a key pathway for plant C allocation that deserves greater
575 empirical and model attention.

4.2 Heterotrophic respiration and microbial growth

Our model identified root exudation as the dominant driver of higher heterotrophic respiration under eCO₂, mainly as rapid microbial respiration of newly supplied labile C. Simulations showed that more than half of the additional root exudation-derived C was directly respired as overflow respiration. Although there is no partitioning in heterotrophic respiration by
580 substrate origin in EucFACE, this result is consistent with other studies showing that under eCO₂, most soil respiration originates from recently fixed C (van Groenigen et al., 2017; Taneva et al., 2006). Microbial CUE was a key modulator of soil C sequestration and respiration (Spohn et al., 2016; Tao et al., 2023, 2025). Simulated annual microbial CUE ranged between 40-% and 50-% and did not change under eCO₂ (Fig. B11). A decline in microbial CUE under greater C supply or nutrient limitation₇ would reduce microbial growth and increase the fraction of root exudates respired (Schimel and Weintraub, 2003).
585 Our results are conservative in that respect but still support the hypothesis₇ that the majority of additional heterotrophic respiration originates from new plant-derived C.

In the model, root exudation disproportionally~~disproportionately~~ stimulated microbial C growth, and consequently gross necromass production, under eCO₂. This suggests that microbes might change their diet under eCO₂ to more easily available and more degradable substrates for C gain (Ai et al., 2023; Dijkstra et al., 2013; Zhou et al., 2021). However, higher gross
590 microbial growth in C₇ also increased microbial nutrient requirements, influencing decomposition and nutrient acquisition processes.

4.3 Microbial nutrient acquisition

Our simulations suggest that, to meet increased nutrient demands under eCO₂, microbes enhanced necromass decomposition and biochemical mineralization; however, observations of enzyme activity only partially support this pattern. For N, demand
595 was met by increased uptake of available inorganic N and decomposition of necromass. Priming of microbial necromass increased, but without a substantial shift in its relative contribution to growth. Here our model partially disagreed with field

630 observations based on soil enzymes: (Pihlblad et al., 2023) found no increase in N-degrading enzymes or microbial nutrient limitations under eCO₂. However, it is questionable if this effect would be statistically detectable in a FACE experiment, with inherently low sample size and difficulties in detecting changes in the soil (Filion et al., 2000).

For P, our model suggests that additional microbial P demand was primarily satisfied by increased biochemical mineralization of organic sources, including necromass. As a consequence, eCO₂ increased available PO₄ by 20% (Fig. B12). This is partially
635 consistent with observations which report increased PO₄ concentrations under eCO₂ in rhizosphere or deeper soil layers (Hasegawa et al., 2016; Ochoa-Hueso et al., 2017; Pihlblad et al., 2023). To our knowledge it is not yet resolved which processes caused the increased PO₄ concentration in EucFACE. In accordance with the model, observations from other ecosystems report increased phosphatase activity under P limitation (Marklein and Houlton, 2012) or under high soil organic P content (Margalef et al., 2017). In EucFACE, eCO₂ caused no significant increase in phosphatase at the start of the
640 experiment (Hasegawa et al., 2016), after 1-1/2 years (Ochoa-Hueso et al., 2017) or after 4-1/2 years (Pihlblad et al., 2023).

Model uncertainties derive from assumptions on nutrient acquisition strategies and root exudation stoichiometry. NH₄ availability and recycling of microbial nutrients ~~en~~ upon microbial turnover strongly contributed to microbial N acquisition under eCO₂, but remain poorly constrained and require further field observations.

645 Additionally, we do not account for P acquisition by increased carboxylate exudation, which could have increased PO₄ concentrations via ligand exchange with Fe-Al-oxides at soil surfaces (Hinsinger, 2001; Wang and Lambers, 2020) and has been reported for common EucFACE understorey species (Hasegawa et al., 2023). We currently lack field observations to implement such mechanisms in the model, and therefore the model resolves enhanced microbial P demand with increased biochemical mineralization.

650 Finally, simulated microbial nutrient demand is substantially controlled by root exudation stoichiometry. In ~~our~~ the model root exudation C-to-N ratio was 176 (no P exudation), whereas microbial C-to-N ratio was 4.3 (N:P = 4.1). Simulated C:N ratio is higher than root exudation measurements (Li et al., 2021; Su et al., 2022; Zhang et al., 2016) but ensures that modelled root exudation does not cause an extensive N loss in plants. As a consequence, increased root exudation enhanced microbial nutrient demand, and plant-microbial competition for N and P (Thurner et al., 2023). Under a root exudation stoichiometry closer to
655 microbial stoichiometry, increased root exudation may further promote microbial growth. Microbial N supply may be less dependent on decomposition of microbial necromass, resulting in stronger decomposition of litter for C acquisition. Instead, a substantial amount of N would be stored in SOM, unavailable, ~~for~~ to plants. Root exudation C:N ratio remains a key variable in plant-microbe nutrient dynamics, but further research regarding the fate of exudate N is needed to improve model assumptions in plant C-for-N trade mechanisms (Drake et al., 2013; Rumeau et al., 2025).

660 4.4 Soil C sequestration

~~Our~~ The model shows that under increased root exudation, microbial growth can simultaneously increase gross necromass ~~gross~~ production and necromass decomposition, resulting in no substantial net effect in soil C storage (Drake et al., 2011; van

Groenigen et al., 2014; Kuzyakov et al., 2019). In ~~our~~the model, priming offset gross necromass production and contributed to increased heterotrophic respiration under eCO₂. There are no continuous measurements from EucFACE analyzing changes in soil organic matter age composition. However, measurements using a combination of litter bag and isotopic signature measuring (Castañeda-Gómez et al., 2020) showed that eCO₂ increased losses of old SOC and input of new SOC at EucFACE
700 in summer months, agreeing with our simulations.

Uncertainties in C storage arise from model representation of C cycling in deep soil layers and mineral sorption of necromass. The model predicts increased soil C in deep soil layers under eCO₂, caused by increased root exudation in these soil layers. As the model assumes root exudation following root biomass distribution, eCO₂ enhances root exudation in deeper soil layers with low microbial activity (Fig. 4). As a consequence, additional labile C is adsorbed to the mineral surface and thereby
705 sequestered. While specific exudation rate may differ with depth and function of roots, we are currently missing data to further calibrate this.

Additionally, necromass is partially protected from decomposition by association with soil mineral surfaces. Our model accounts for this process but we are lacking measurements for site-specific sorption capacity and affinity. Less mineral protection would translate ~~into~~ stronger microbial necromass cycling, as the simulated depolymerization flux depends on
710 availability of decomposable material. Further, the model simulates increased desorption of mineral-associated necromass under eCO₂. This is partly caused by additional root exudation competing with necromass for sorption sites, but also by model assumptions about the amount of available mineral soil sorption sites with increasing organic matter and litter. This model assumption increased microbial-available N-rich material and may have enhanced the ~~eCO₂~~eCO₂ effect on necromass decomposition in the model.

715 We further simulated small shifts in P pools from slow cycling microbial necromass to fast cycling microbial biomass (< 2% change in necromass). A recent analysis of the P budget for EucFACE showed that eCO₂ treatment led to no significant changes of soil organic P pools (Jiang et al., 2024b), but changes of this magnitude are likely below the detection limit of field observations.

4.5 Comparison to other models

720 Implementing root exudation in QUINCY-JSM improved the predicted CO₂ response of C allocation, but results still indicate that further development is necessary. A recent model inter-comparison study demonstrated that most C-N-P cycle models, including QUINCY-JSM, overestimate the ecosystem C sequestration of the EucFACE ecosystem under eCO₂ (Jiang et al., 2024a). In contrast to observations, most models simulated a positive effect on net ecosystem productivity (NEP) under eCO₂. Additionally, all, ~~except one model,~~ allocated most additional C fixed under eCO₂ to either autotrophic respiration, storage or
725 structural biomass, and underestimated the increase in soil heterotrophic respiration. The exception was GDAYP, which implemented root exudation but no microbial dynamics.

Implementing root exudation improved the allocation of additional GPP: Compared to other models in Jiang et al. (2024a) and to QUINCY-JSM without root exudation, and consistent with observations, QUINCY-JSM with root exudation reproduces

730 ~~the increase in C respired via~~ allocates a substantial part of additional GPP to heterotrophic respiration ~~and the decrease in C~~
~~lost through~~ instead of autotrophic respiration. Additionally, less C remains in the system in the form of increased vegetation
pools (Fig. B8). With consideration of root exudation, the model explains weak ~~responses~~ increases in topsoil C ~~tounder~~ eCO₂
by respiration of root exudation and priming, rather than by low litter C input (Fig. B9).

735 Implementing root exudation improved the simulated CO₂ response in heterotrophic respiration, but not in NEP, due to the
effect on BP and deep soil C accumulation. Regardless of root exudation, QUINCY-JSM simulates increased net P
mineralization under eCO₂. Therefore, it remains difficult to evaluate the actual effect of the implementation on PO₄
mineralization. Further model adjustment is needed to fully understand the feedback of plant-microbe interactions on plant
nutrient uptake under eCO₂.

4.6 Suggestions for further advancements in modelling and experimental work

740 In the following, we provide methodological directions for upcoming FACE experiments and terrestrial biosphere models, to
improve understanding of root exudation and microbial representation under eCO₂.

4.6.1 Soil Phosphorus limitation

FACE experiments suggest a strong interaction between nutrient limitation and CO₂ fertilization effect, but it remains uncertain
how effectively current models represent nutrient limitation (Fleischer et al., 2019; Jiang et al., 2024a; Zaehle et al., 2014).
745 The simulated, but not observed, ~~response of increase in~~ BP, suggests that our model underestimates P limitation on plant
growth under eCO₂. Overestimation in P pools may be solved with alternative model initialization approaches, assisted by
Hedley fractions to determine P extractability in soils (Hedley et al., 1982; Helfenstein et al., 2024).

We suggest future model development should consider improved representation of sorption dynamics (Yu et al., 2023) and
site-specific soil properties, namely pH or Fe-Al-oxides ~~on them~~ (Wang et al., 2022). Aspects like C or N cost ~~for of~~
biochemical mineralization, accessibility of mineral-associated material for phosphatase or plant competitiveness against
750 microbes need further investigation but currently lack data for parameterization.

4.6.2 Modelling dynamic root exudation

Global mean rates of root exudation can be benchmarked against broad meta-analysis such as Chari et al. (2024) but further
data ~~is~~ are needed to constrain root exudation variability (Brunn et al., 2022; Hasegawa et al., 2023). In the context of
atmospheric CO₂ increase on ~~the~~ ecosystem level, direct measurements used, for example, in ~~BioFACE~~ BioFACE or
755 ~~DukeFace~~ Duke FACE (Drake et al., 2011; Reay et al., 2025) provide reliable data for model evaluation. Such measurements
should consider upscaling into ecosystem level, e.g., annual flux per unit land area, implying a scaling by other observables
such as root mass or soil volume (Norby et al., 2024), and seasonal changes ~~of in~~ root exudation (Brunn et al., 2025; Leuschner
et al., 2022; Phillips et al., 2008; Zhang et al., 2022).

760 Additionally, nutrient fertilization experiments (Ataka et al., 2020) or measurements along nutrient gradients (Jiang et al., 2022; Meier et al., 2020) help unravel the relationship between plant nutrient and C surplus status, and root exudation, to constrain model parameters.

4.6.3 Representation of soil microbial organisms

765 Uncertainty arises from parameterization and representation of microbial pools. Currently, only a few ecosystem models implement microbes explicitly (QUINCY-JSM (Yu et al., 2020); OCHDX (Zhang et al., 2020); CLM5-MIMICS-CN (Wieder et al., 2015)). In these models, CUE is a key parameter as it determines how much C initially enters the microbial cycle. In QUINCY-JSM, CUE is dynamically determined by the microbial nutrient imbalance, to represent microbial community changes. Other modelling approaches explicitly represent distinct decomposer pools, to account for changes in turnover or stoichiometry (Zhang et al., 2020). Increased root exudation under eCO₂ may increase bacterial priming or benefit fungal communities (Chertov et al., 2022; Sistla et al., 2014). ~~But~~However, further field studies are required to evaluate how 770 community changes control soil C storage and respiration.

Additional uncertainty comes from the role of mycorrhizal associations under eCO₂ (Terrer et al., 2016). We assume that mycorrhizal activity and C allocation to mycorrhizal community are covered by a general microbial pool and root exudation flux. We thereby neglect variations in plant nutrient acquisition strategies (Reay et al., 2025; Talbot et al., 2008; Wen et al., 2022) but reduce the amount of additional parameters. Field experiments need to further quantify C allocation to mycorrhiza- 775 to estimate total plant belowground C allocation. However, implementation of mycorrhiza in TBMs remains a subject of ongoing debate regarding necessary mechanisms and model simplifications (Turner et al., 2023).

4.6.4 Priming effects and soil organic matter decomposition

Our model emphasizes the role of necromass decomposition and mineralization for nutrient acquisition, but identifying control mechanisms requires further model and field experiments. Priming effects depend on N availability and demand controlled by 780 input stoichiometry. While priming effects were small in our simulations, they may play a more prominent role in N-limited systems, potentially reducing long-term soil C sequestration.

In comparison to most other models, which directly prescribed priming (Jiang et al., 2019; Turner et al., 2023), representing priming effects as emergent, ~~microbial-microbially~~ mediated processes ~~allow~~allows the analysis of underlying processes. However, most ecosystem models currently lack representation of this process (Jiang et al., 2024a; Walker et al., 2015).

785 In field experiments, artificial root exudates can be used to simulate the effect of additional input of labile C into soils and produce evaluation output for models (Lopez-Sangil et al., 2017). Future research should focus on the influence of different soil properties, such as pH and nutrient status (Bastida et al., 2019; Spohn et al., 2013; Sun et al., 2019) and feedback on plant nutrient availability.

5. Conclusion

790 In this study, we implemented a dynamic root exudation mechanism in a nutrient-enabled terrestrial biosphere model, and demonstrated that this process substantially improved the plant C allocation responses to eCO₂ in a mature forest FACE experiment. A key insight from our analysis is that root exudation, as a largely hidden pathway, provides a mechanistic link between increased GPP and heterotrophic respiration observed under eCO₂, thereby explaining why soil C storage in EucFACE remained largely unchanged despite greater C inputs. Our results further demonstrate that explicit coupling between root exudation, microbial activity, and nutrient acquisition is essential for capturing plant-soil feedbacks in nutrient-limited forests. 795 We therefore recommend further development in explicit representation of root exudation, microbial dynamics and plant-microbe interactions to account for these effects in global models. Strengthening empirical data ~~on ecosystem scale~~ exudation and microbial responses in FACE experiments at the ecosystem scale will be essential to reduce uncertainty.

Appendix

800 To improve simulations under ambient conditions, we calibrated several parameters in QUINCY-JSM for simulations of
EucFACE (Table A1). Additionally, we changed processes in microbial decay to allow for priming effects in QUINCY-JSM
and altered inorganic soil P initialization for deeper soil layers to account for highly weathered soils in EucFACE. To account
for low P levels in subsoils of deeply layered soils, we simulate an exponential decline in initial inorganic P pools (assoc_slow,
occluded, primary, solute and assoc_fast) below ~~70~~70 cm depth.

805

A1 Calibrated Parameters

Table A 1: Parameters changed in QUINCY-JSM for EucFACE simulation

parameter	description	unit	QUINCY-JSM standard	This study	reference/reason for change
soil					
microbial_cue_max	Maximal microbial carbon use efficiency	[unitless]	0.6	0.5	Adjust to meet microbial biomass in EucFACE
k_slow_som_np	N:P ratio for microbial necromass pool initialization	g g ⁻¹	14	21	Reduce P in system
Microbial_cn	Microbial N:C ratio	g g ⁻¹	7.6	4.3	Pihlblad et al., 2019
Microbial_np	Microbial N:P ratio	g g ⁻¹	5.6	4.1	Pihlblad et al., 2019; Jiang et al., 2020; Jiang et al., 2024
Qmx_org_fp	maximum sorption capacity	molC (kg fine particle) ⁻¹	6.5537	5.57	Reduce organic matter sorption to

	of OM to fine soil particle				account for soils at EucFACE
km_mic_biochem_po4	Half-saturation microbial biomass for PO ₄ biochemical mineralization	molC m ⁻³	0.42	12.49	Account for P-limited soils
vegetation					
Jmax2vcmax_C3	ratio of Jmax25/Vcmax25 for prescribed leaf N	[unitless]	1.92	1.64	Jiang et al., 2024
Root2leaf_cn	relative C: N of fine roots compared to leaves	[unitless]	0.85	0.62	Jiang et al., 2024
lambda_sinklim_PS	Weibull parameter for sink limitation	[unitless]	0.1	0.05	Reduced sink limitation to allow for root exudation
Wood2leaf_cn	relative C: N of sapwood biomass compared to leaves	[unitless]	0.145	0.32	Jiang et al., 2024
Root2leaf_np	relative N:P of fine roots compared to leaves	[unitless]	0.8	1.0	Jiang et al., 2024
Wood2leaf_np	relative N:P of sapwood biomass compared to leaves	[unitless]	0.64	1.0	Jiang et al., 2024

SLA	specific leaf area	mm (mg DW) ⁻¹	8.99	6.01	Jiang et al., 2024
K_crtos	coarse root to sapwood mass ratio	[unitless]	0.4	0.1	Jiang et al., 2024
K_rtos	trade-off parameter for hydraulic investment into sapwood or fine roots	[unitless]	5.615	4.925	Adjusted to follow allocation in Jiang et al., 2020
K_latosa	leaf area to sapwood area ratio	[unitless]	4000	3000	Adjusted follow allocation in Jiang et al., 2020
Tau_fine_root	fine root turnover	yr	0.75	1.5	Jiang et al., 2024

A2 Enabling priming via microbial grazing

810 When microbes decay, in the model part of biomass is directly recycled as DOM, part enters the necromass pool. We altered microbial decay, such that for nitrogen an additional part enters solute NH₄ to account for microbial grazing. ~~Original~~The original JSM describes element transfer upon microbial turnover as:

~~$$\eta_{mic \rightarrow dom}^x = \sigma_{recycle}^x * \frac{X_{mic}}{\tau_{mic}} \quad (A1)$$~~

$$\eta_{mic \rightarrow res}^x = 1 - \eta_{mic \rightarrow dom}^x \quad (A2)$$

815 Where $\eta_{mic \rightarrow dom}^x$ [molX m³ s⁻¹] and $\eta_{mic \rightarrow res}^x$ [molX m³ s⁻¹] are the fluxes from microbial pool to DOM and necromass pool, respectively, X_{mic} [molX m³] is the microbial pool and τ_{mic} [s] is the microbial turnover time for C, N and P. $\sigma_{recycle}^x$ [unitless] is a constant recycling fraction for C and P, but flexible for N. Under N limitation microbes recycle up to 66% of N, depending on microbial nutrient status. Therefore, microbes in need ~~for~~of N under additional growth would increase recycling but not change enzyme allocation. To bypass this, we fixed the recycling factor and simulate the effect of microbial grazing as:

$$\eta_{mic \rightarrow dom}^N = \sigma_{recycle}^N \cdot \frac{N_{mic}}{\tau_{mic}} \quad (A3)$$

$$\eta_{mic \rightarrow NH_4sol}^N = \sigma_{grazing}^N \cdot \frac{N_{mic}}{\tau_{mic}} \quad (A5)$$

$$\eta_{mic \rightarrow NH_4sol}^N = \sigma_{grazing}^N \cdot \frac{N_{mic}}{\tau_{mic}} \quad (A5)$$

$$\eta_{mic \rightarrow res}^N = 1 - \eta_{mic \rightarrow dom}^N - \eta_{mic \rightarrow NH_4sol}^N \quad (A6)$$

825 Where $\eta_{mic \rightarrow NH_4sol}^N$ [molX m³ s⁻¹] is the grazing flux from microbial pool to soluble NH₄ pool and $\sigma_{grazing}^N$ [unitless] is the related fraction.

Table A 2: New parameters for microbial decay and recycling

	Unit	Standard Quincy-JSM	This study
$\sigma_{recycle}^C$	unitless	0.172	0.3
$\sigma_{recycle}^N$	unitless	(0.172–0.66), At least 0.6 if microbes under N limitation	0.4
$\sigma_{recycle}^P$	unitless	0.172	0.5
$\sigma_{grazing}^X$	unitless	-	0.2

Table B 1: Comparison of mean annual of simulated pools (gC m⁻²) and fluxes (gC m⁻² yr⁻¹) for EucFACE under ambient conditions with observed means and \pm one standard deviation across 3 rings (2013-2016). NEP refers to 3 different alternative methods of estimation (Jiang et al., 2020; Jiang et al., 2024a)

Carbon pool (gC m⁻²)	observed	simulated
Leaf	151 (\pm 14)	145
Wood	4558 (\pm 321)	4218
Fine root	227 (\pm 5)	182
Coarse root	606 (\pm 60)	622
Soil carbon	2.183 (\pm 280) (top 10 cm)	2456(top 13 cm)
Microbial carbon	61 (\pm 3.6)	81
Carbon flux (gC m⁻² yr⁻¹)	observed	simulated
Overstorey GPP	1563 (\pm 200)	1702
NEP	-73 \pm 28	1
Biomass production	484 (\pm 63)	365
Soil respiration	1097 (\pm 86)	1207

Table B 2: Comparison of mean annual of simulated pool stoichiometry for EucFACE under ambient conditions with observations (2013-2016) (Jiang et al., 2024a)

Variable	Observed CN	Simulated CN	Observed NP	Simulated NP
leaf	35.5 \pm 2.7	29.6	22.9 \pm 0.1	24.4
sapwood	101.6 \pm 14.7	110.9	35.6 \pm 2.1	35.8
wood	110.2 \pm 30.3	138.7	33.7 \pm 2.7	35.8
fineroot	56.9 \pm 4.6	47.7	28.7 \pm 3.3	30.5
soil	13.8 \pm 1.0	11.9	16.4 \pm 3.4	16.2

840

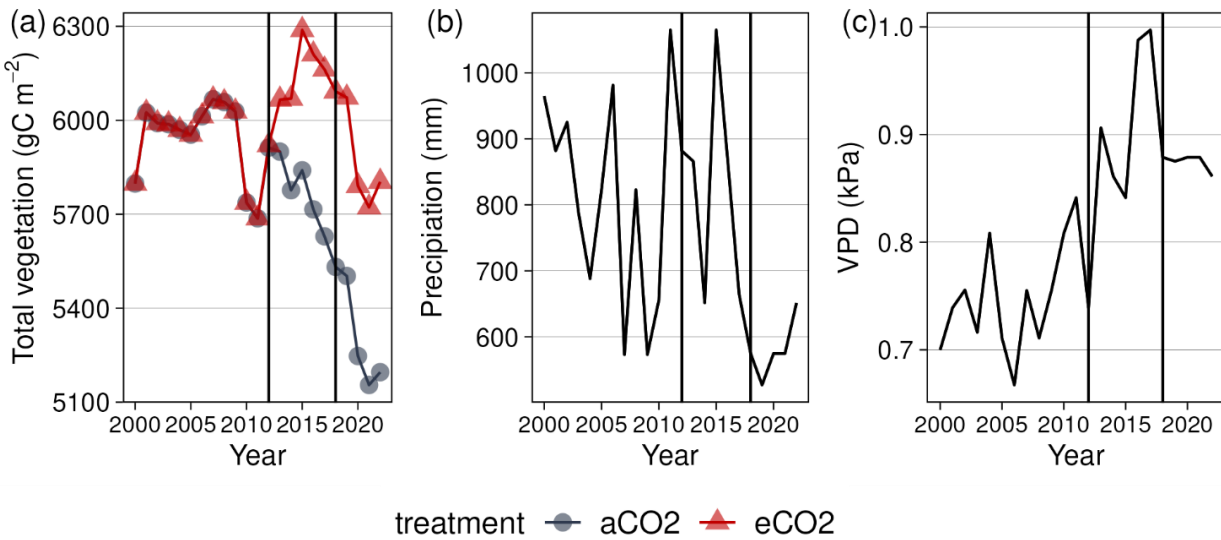
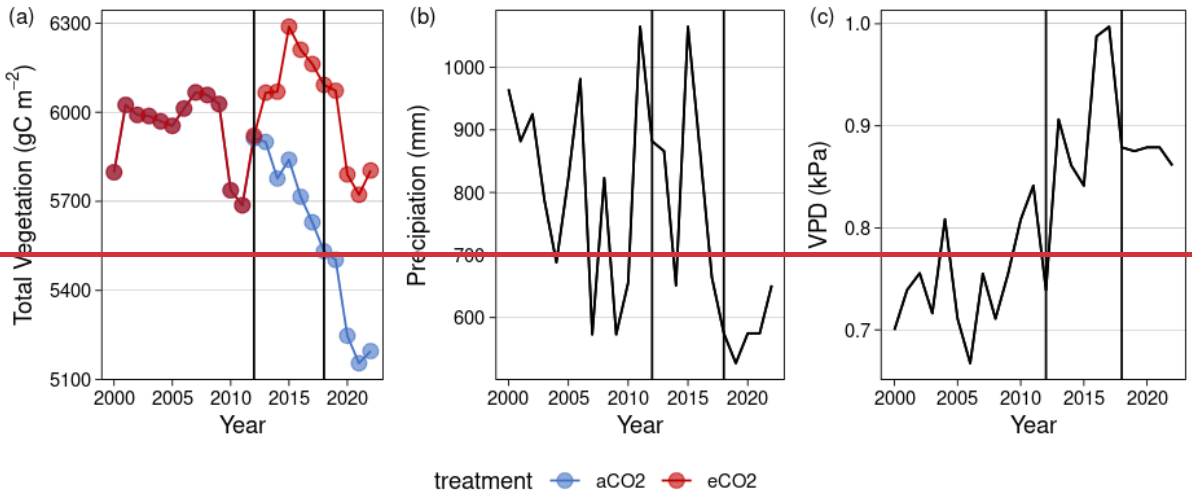
Table B 3: Observed (2013–2016) and simulated (2013–2019) CO_2 effect on ecosystem fluxes at EucFACE. Our model did not include understorey. Observed values refer to overstorey gross primary productivity (GPP), biomass production on aboveground overstorey and whole vegetation root biomass production (BP), autotrophic respiration on aboveground overstorey and whole vegetation root respiration (Autotrophic respiration), heterotrophic respiration and soil respiration. Observed values from Jiang et al 2020.

Carbon Flux	Observed increase	Simulated increase
Overstorey GPP	12-%	22-%
Biomass production (BP)	3-%	33-%
Autotrophic respiration	5-%	13-%
Heterotrophic respiration	17-%	14-%
soil respiration	12-%	13-%

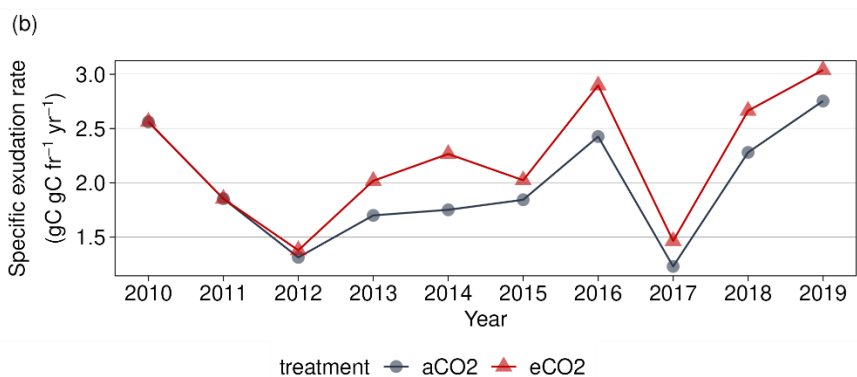
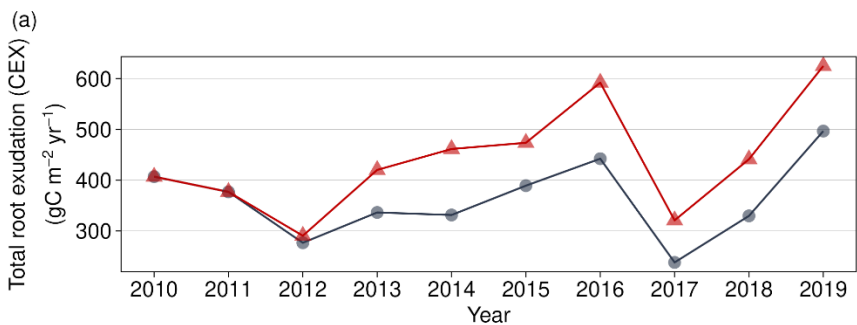
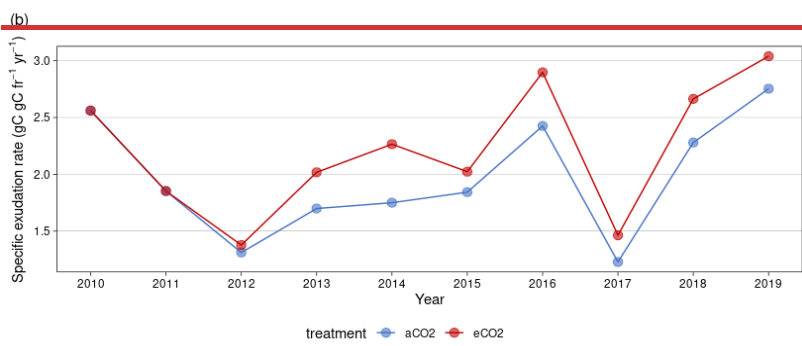
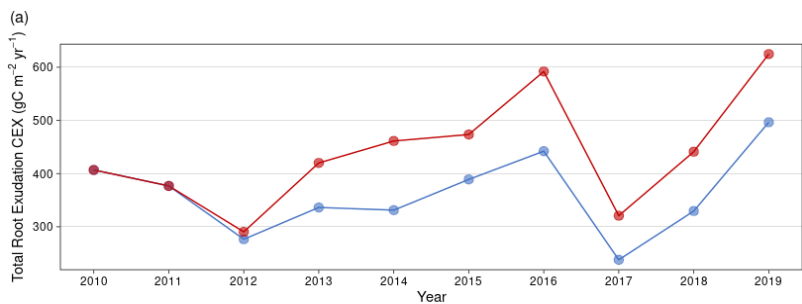
845

Table B 4: Modelled turnover times under ambient and elevated CO_2 for the ecosystem (C), soil (C, N, P) and microbial necromass (C, N, P). Calculated for 2015–2019.

		$\tau_{soil}(yr)$	$\tau_{necromass}(yr)$
carbon	aCO ₂	17.1	30.4
	eCO ₂	15.1	27.7
nitrogen	aCO ₂	242.1	30.5
	eCO ₂	193.2	27.7
phosphorus	aCO ₂	561.2	8.2
	eCO ₂	447.6	6.4

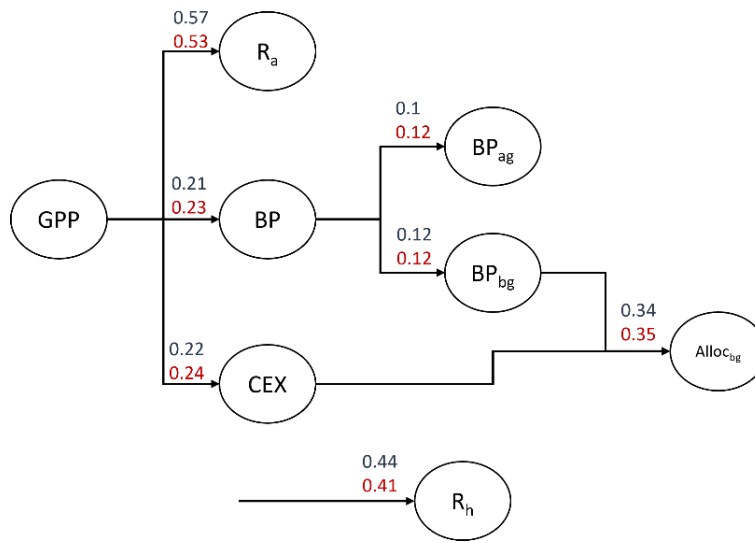
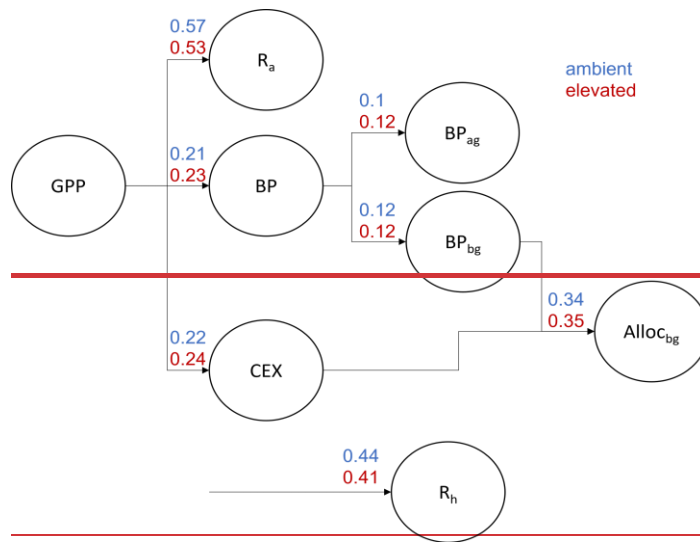


850 **Figure B-1B1:** Simulated total vegetation C, precipitation and vapor pressure deficit (VPD) from 2012 to 2022 for EucFACE under ambient conditions. Vegetation follows a downward trend from 2010–2022 due to climate extremes. Forcing from 2012-2018 (black bars) follows meteorological data observations, while forcing before and after this period follows repeated and randomized observations.

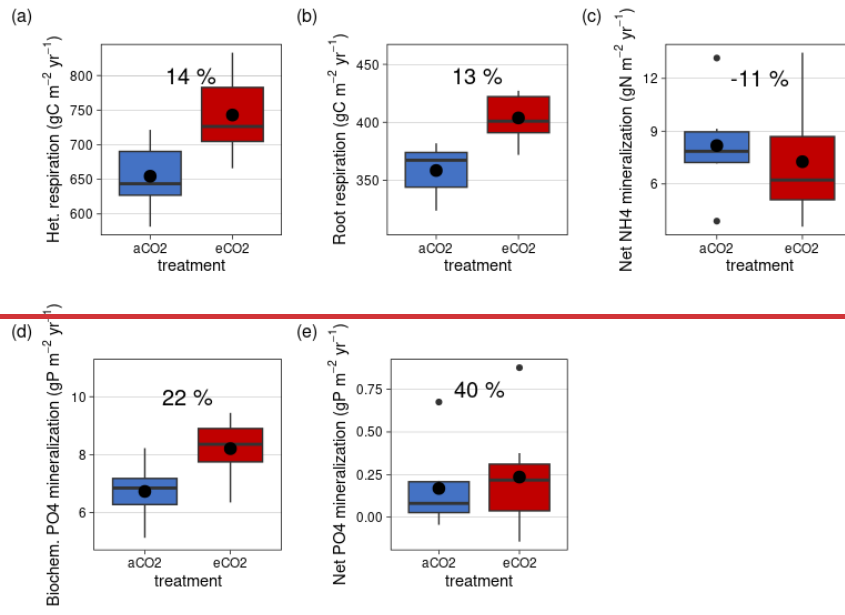


855

Figure B-2B2: Simulated total root exudation for 2010 to 2019 for EucFACE for ambient and elevated treatment as (a) Total root exudation flux and (b) Specific root exudation rate. CO₂ fumigation started with a ramp-up at the end of 2012.



860 **Figure B-3B3:** Simulated allocation of GPP under ambient and elevated CO₂ treatment for EucFACE based on simulated annual mean of fluxes from ~~2012-2013~~2019. Numbers on arrows refer to the fraction of GPP allocated to fluxes. GPP is allocated to autotrophic respiration (R_a), biomass production (BP), including aboveground (BP_{ag}) and belowground (BP_{bg}) biomass production and carbon root exudation (CEX). CEX and BP_{bg} add up to total belowground allocation- (AlloC_{bg}). Additionally, the fraction of GPP that is respired via heterotrophic respiration (R_h) is shown.



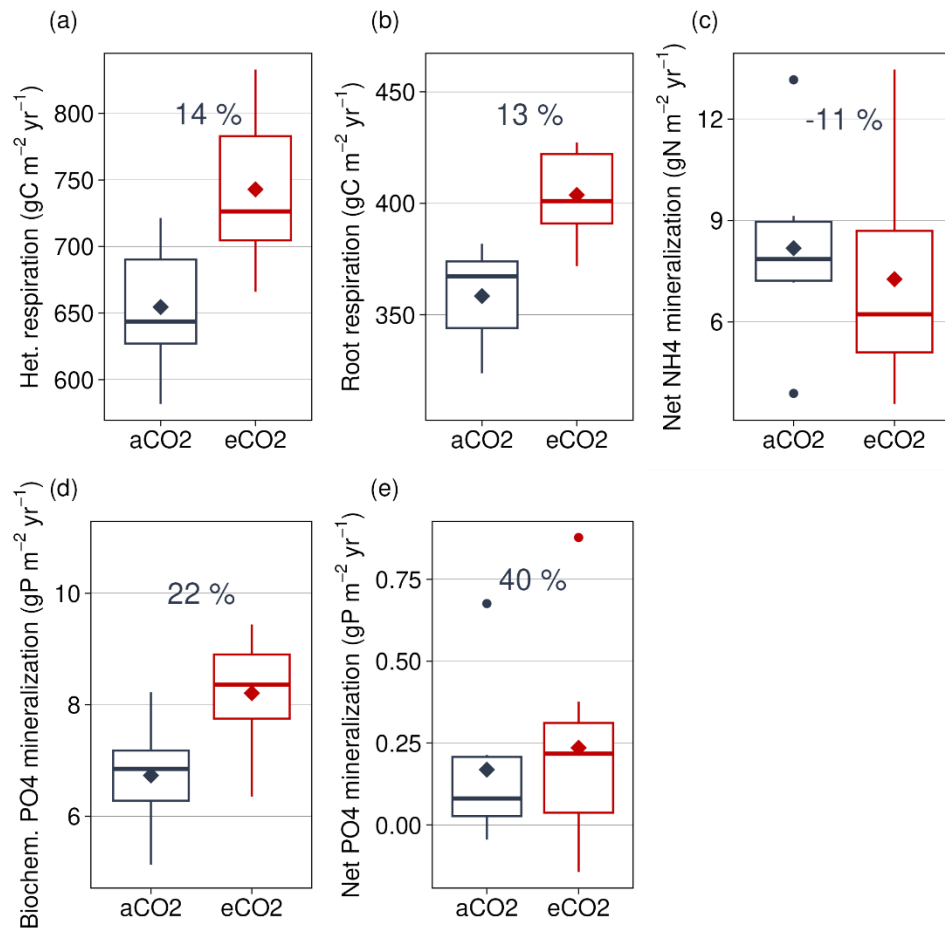
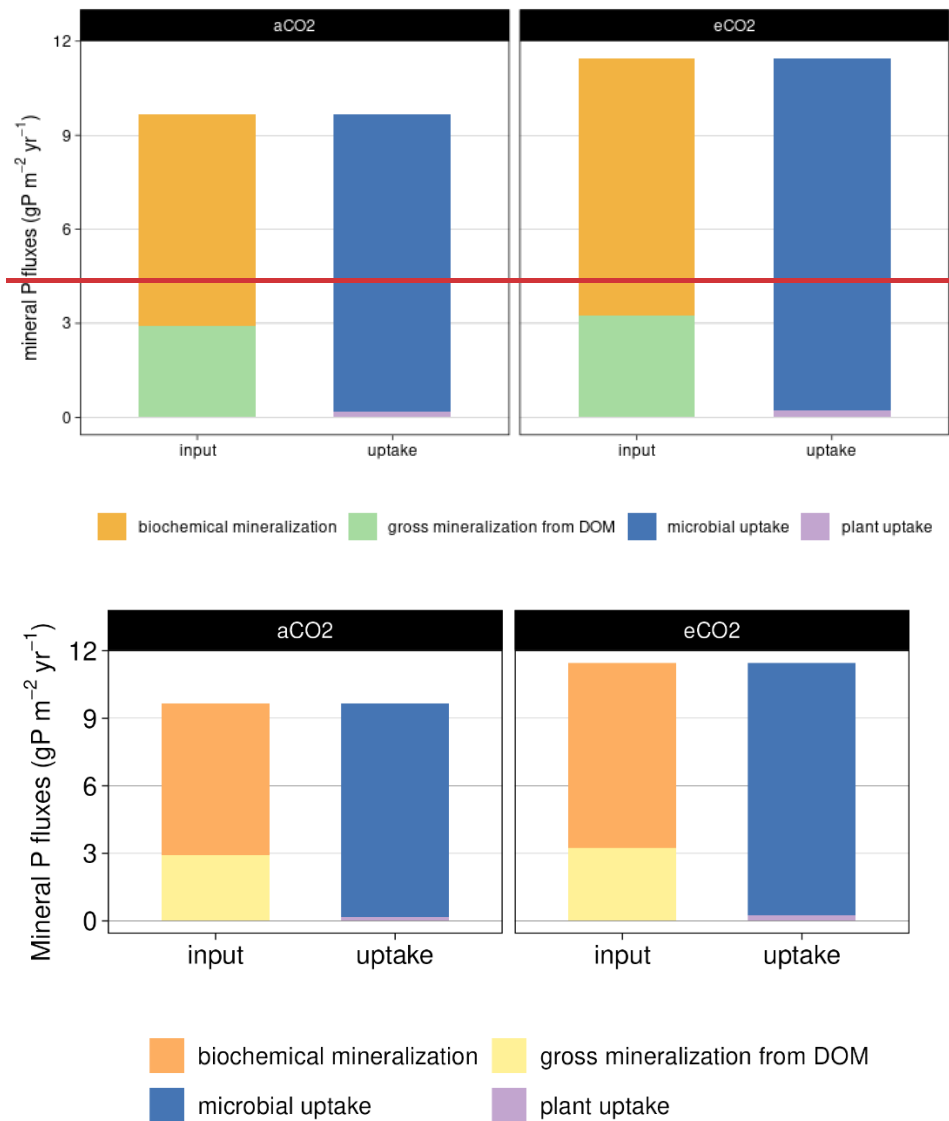
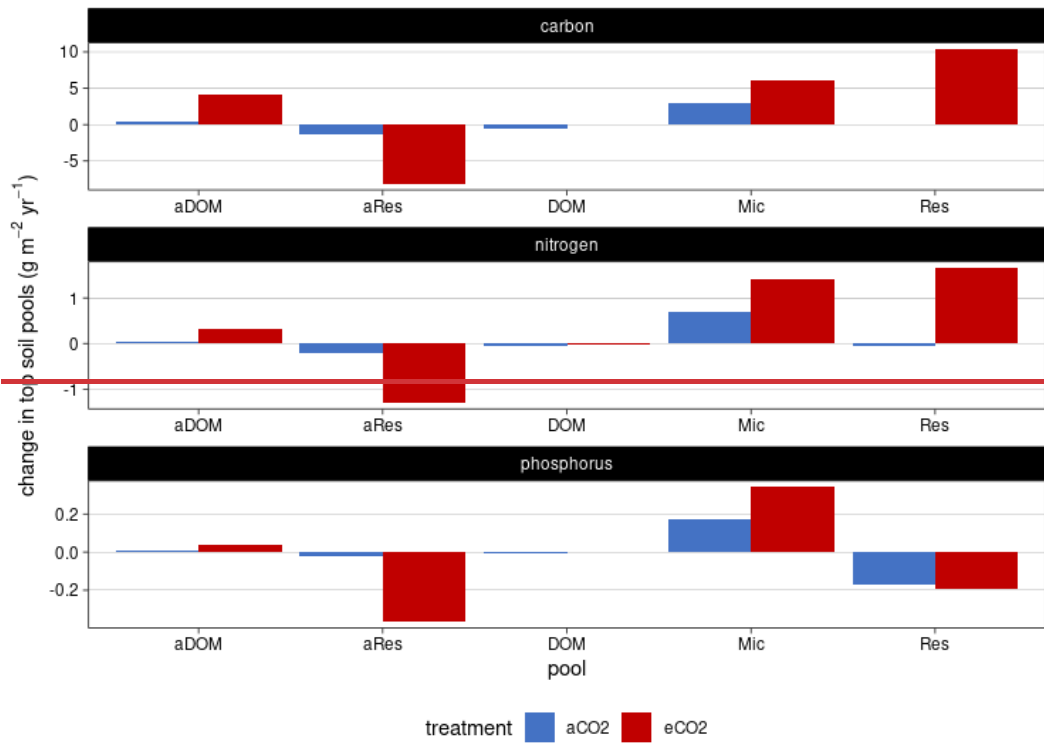


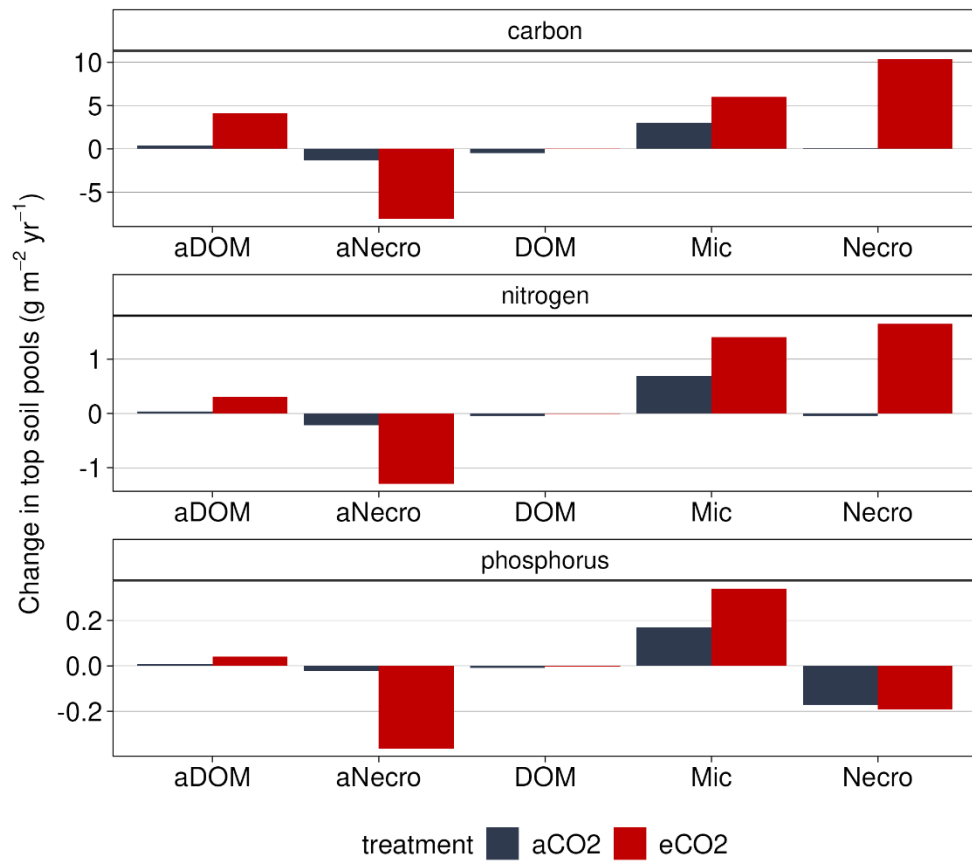
Figure B-4B4: Simulated major mineralization fluxes for C, N, and P under ambient and elevated CO₂ (2013–2019) for topsoil layers. (a) Heterotrophic respiration, (b) Root respiration, (c) Net NH₄ mineralization, (d) biochemical mineralization, (e) Net net PO₄ mineralization as sum of biological and biochemical mineralization. Boxplots show annual variation of fluxes, ~~dots~~rectangles represent mean values. Percentage difference based on ~~Annual~~annual mean for 2013–2019 is given for each flux.

870



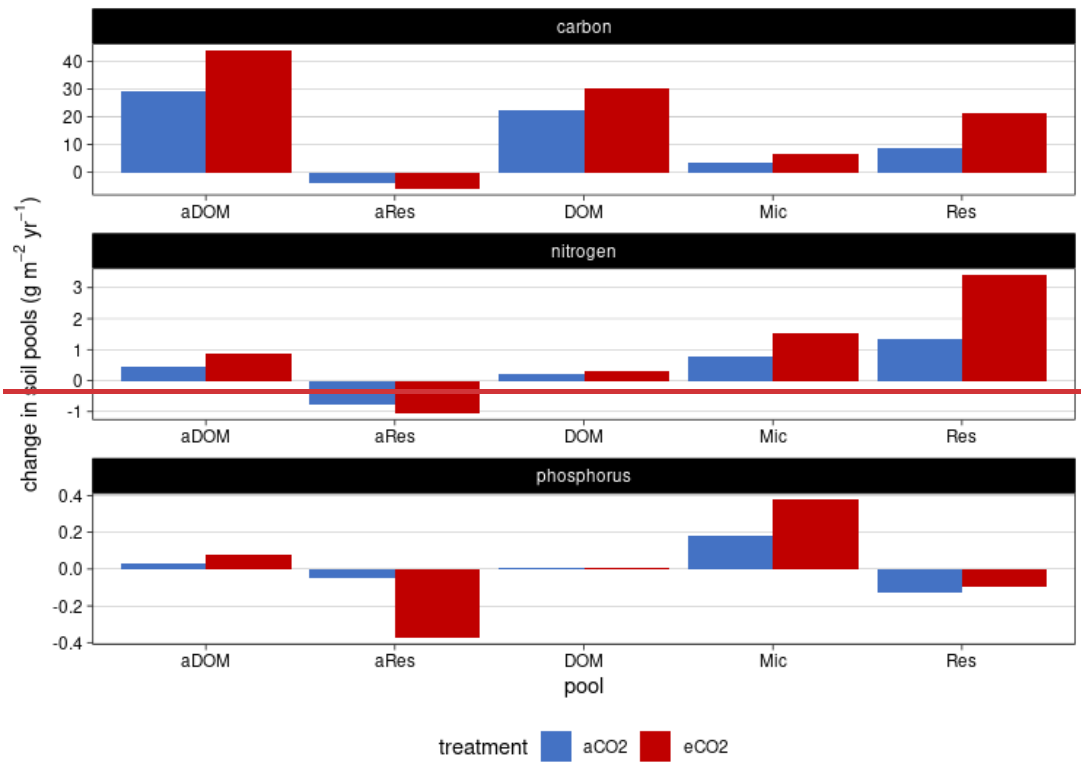
875 **Figure B-5 simulatedB5: Simulated** mineral P fluxes in topsoil layers (50cm50 cm) for ambient (aCO2) and elevated (eCO2) treatment. Annual average from 2013–2019 fluxes which provide (input) plant- and microbes-microbe-available mineral P are gross biological mineralization from DOM and biochemical mineralization. Available P is immobilized via uptake by microbes or plants.

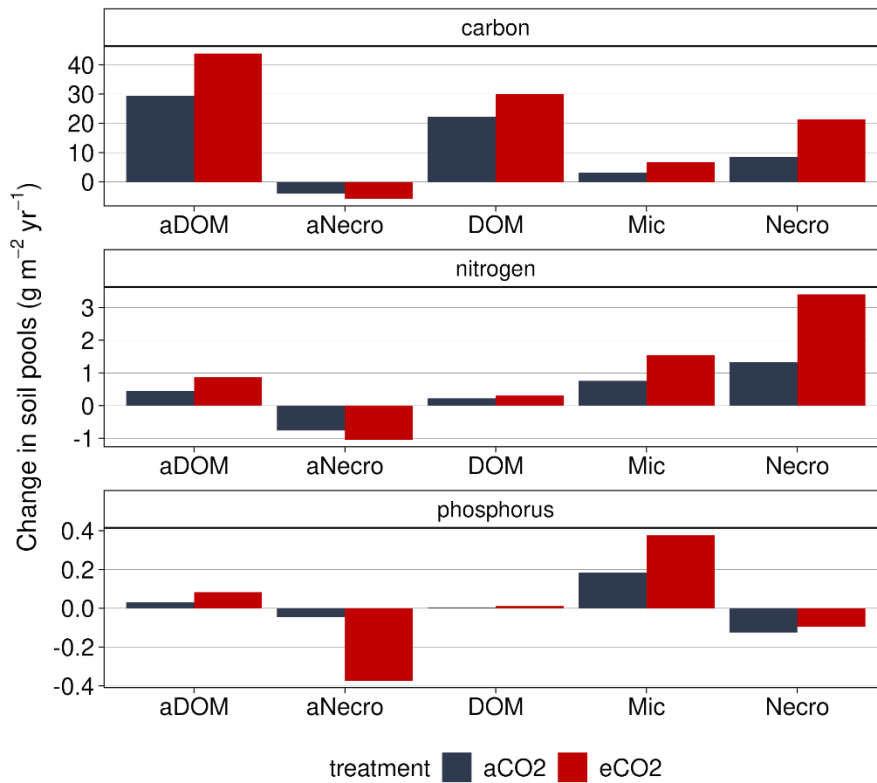




880

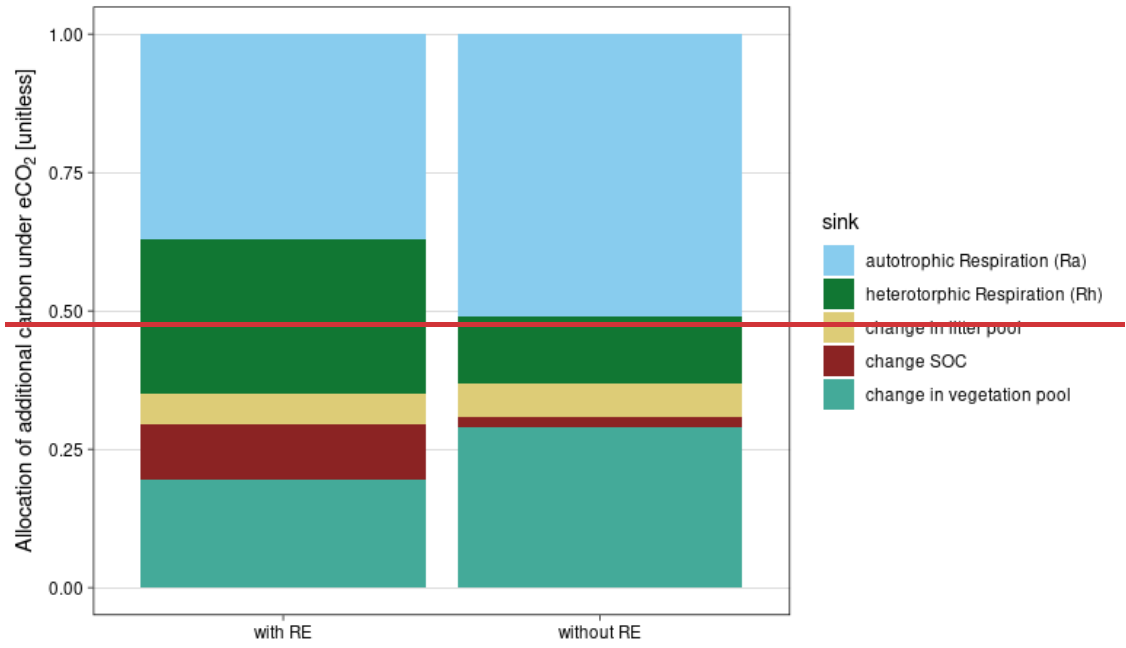
Figure B-6B6: Simulated changes in topsoil pools for EucFACE under ambient and elevated CO₂ treatment 2013–2019: mineral-associated DOM (aDOM), mineral-associated microbial necromass (aNecro), dissolved organic matter (DOM), microbes (Mic) and microbial necromass (Necro).

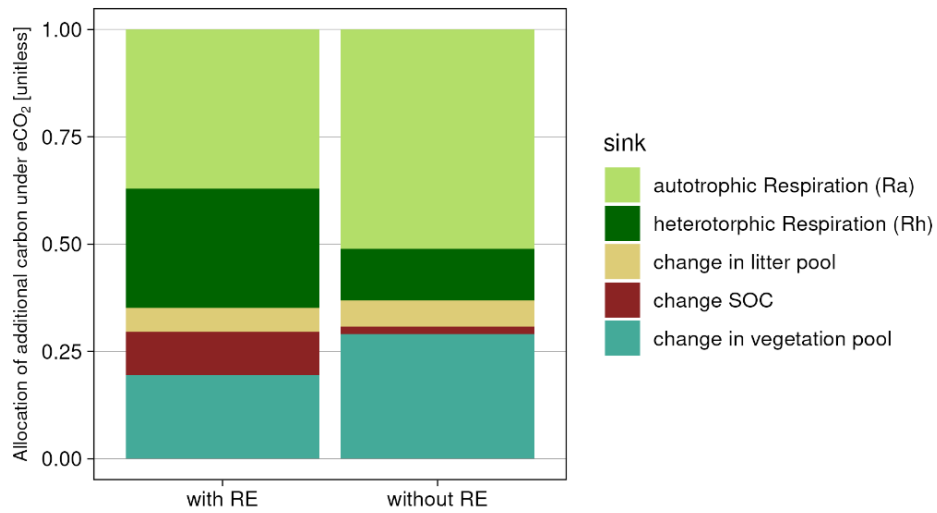




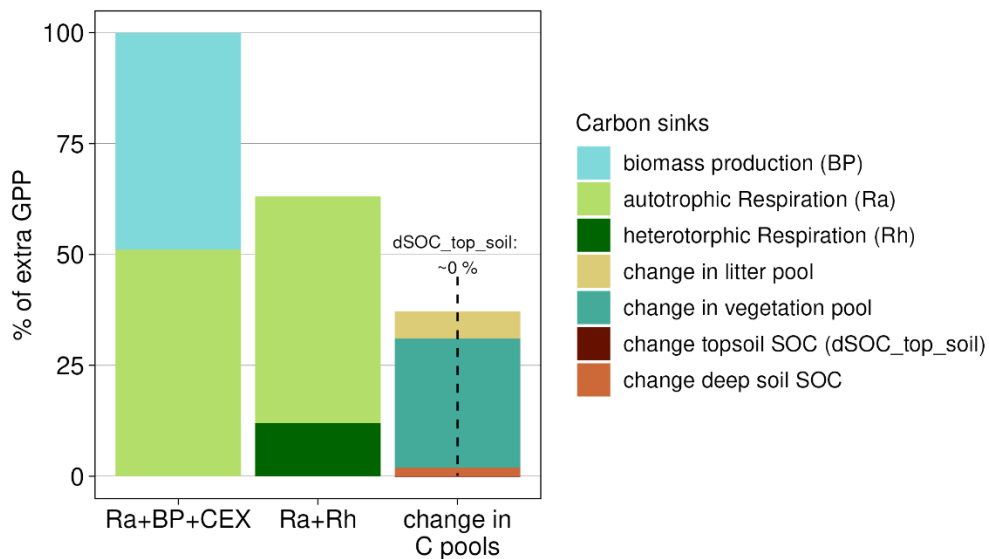
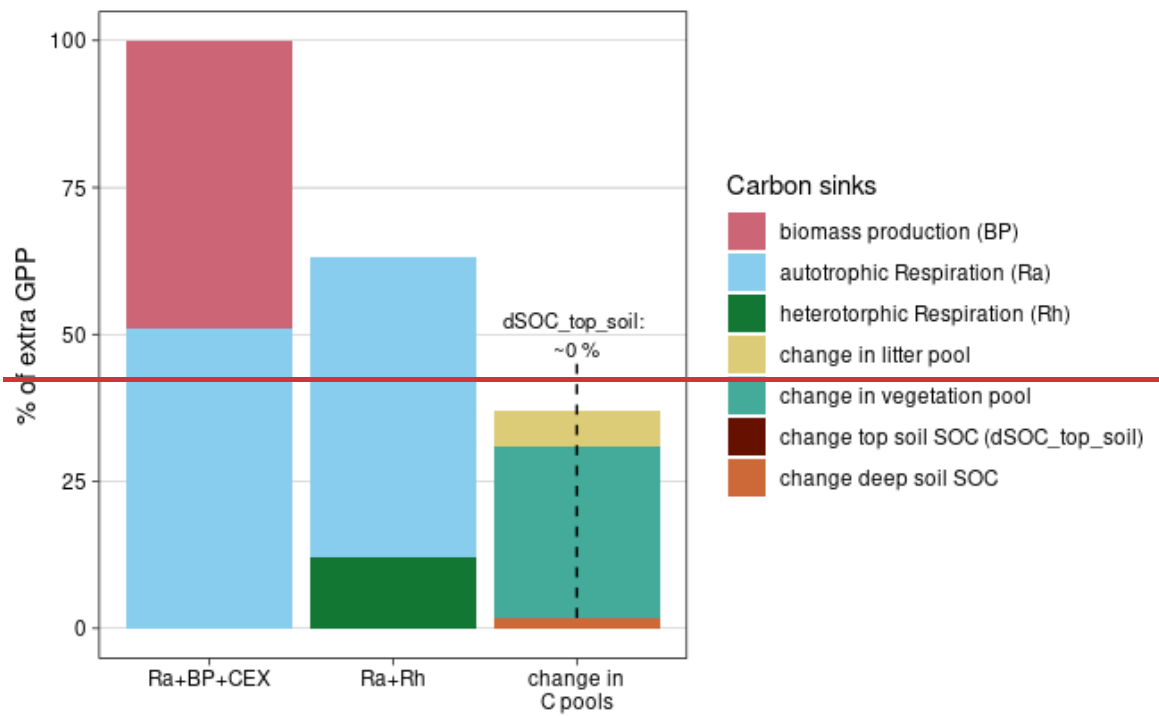
885

Figure B-7B7: Simulated changes in soil pools for whole soil column for EucFACE under ambient and elevated CO₂ treatment 2013–2019: mineral-associated DOM (aDOM), mineral-associated microbial necromass (aResaNecro), dissolved organic matter (DOM), microbes (Mic) and microbial necromass (ResNecro)



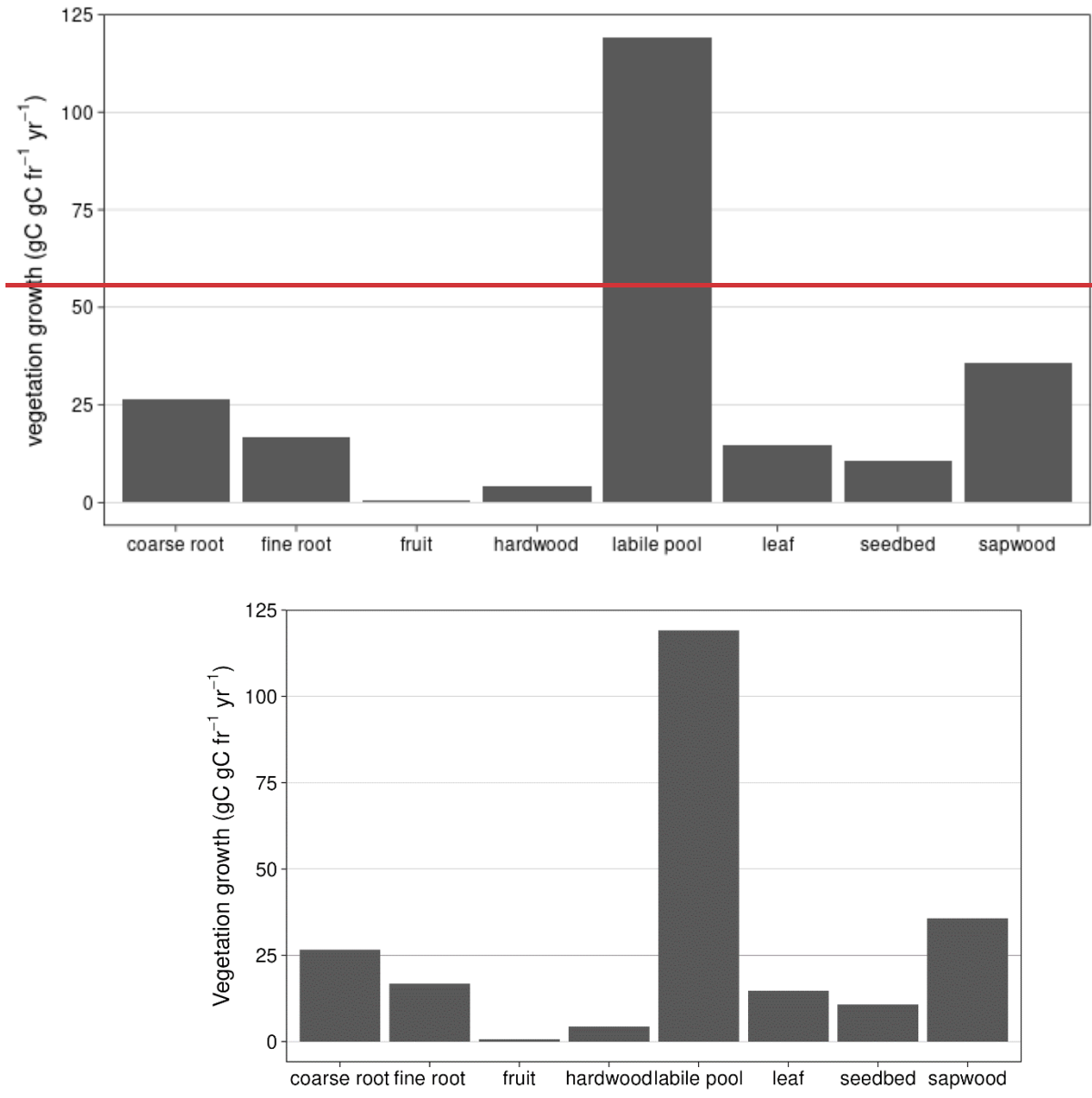


895 **Figure B-8B8:** Simulated allocation of additional GPP under eCO₂ with root exudation module (with RE) and without root exudation module (without RE) for 2013-2029-2019. Additional GPP can be allocated into ~~autotroph~~autotrophic respiration (Ra), heterotrophic respiration (Rh), litter (dlitter), soil organic carbon (dSOC) or vegetation carbon (dVeg₊).



900 **Figure B-9B9:** Simulated fate of additional sequestered C under eCO₂ as percentage of increased overstorey gross primary productivity (GPP) for simulations without root exudation implementation (2013–2019). For simulations, additional GPP is transferred into autotrophic respiration (Ra) and biomass production (BP). Ecosystem respiration (R) is composed of heterotrophic

910 respiration (Rh) and autotrophic respiration (Ra). ~~Change in ecosystem carbon~~ The change in ecosystem carbon pools is composed of change in topsoil organic C ($dSOC_{top\ soil}$ ~~top 10 cm for observation, top 50 cm for simulation~~), change in deep soil SOC ($dSOC_{deep\ soil}$, ~~no observations~~), change in litter ($dLitter$) and change in vegetation ($dVeg$).



915

Figure B-10B10: Simulated mean annual vegetation growth response in different plant pools to eCO₂ from 2013-2019.

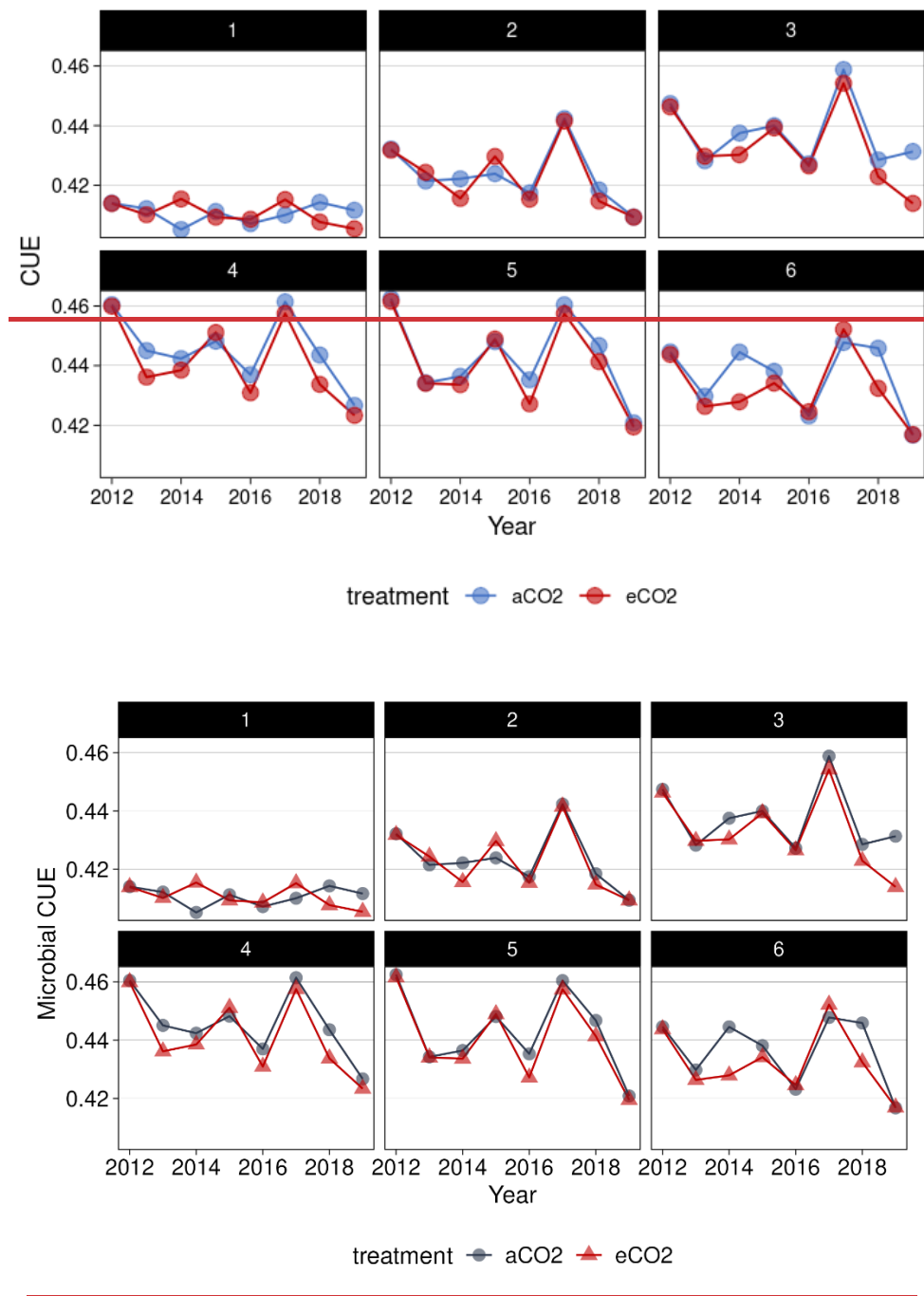


Figure B-14B11: Simulated microbial carbon use efficiency for top six soil layers (topsoil) in QUINCY-JSM JSM for EucFACE under ambient and elevated CO₂ conditions (2013–2019).

920

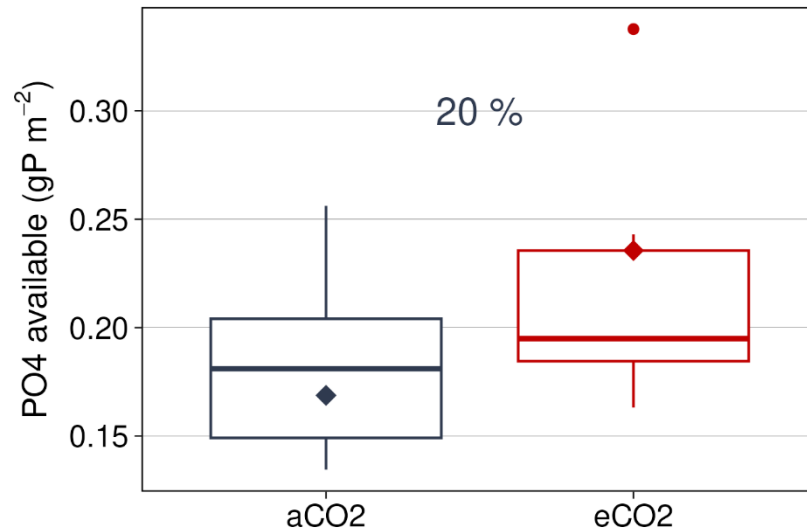
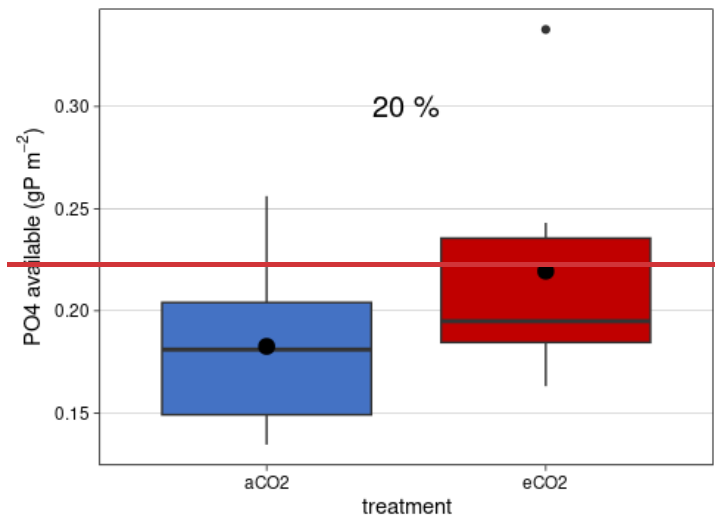


Figure B-12: MeanB12: Simulated mean annual available PO_4 for plant and microbial uptake under ambient and elevated conditions in topsoil for 7 years of simulation (2013–2019). Boxplots show annual variation of fluxes, dots/rectangles represent mean values. Percentage difference based on annual mean for 2013–2019 is shown above boxplots.

925

950 **Code availability.** The model is open source under the GNU GPL vs3 and MPI-M ICON software license agreement (depending on module). The code is available under <https://doi.org/10.17871/quincy-model-2019>. A copy of the scientific code can be found in ~~this temporary (01.12.2025) private link for review purposes:-~~ <https://git.bgc-jena.mpg.de/quincy-model/qs-open-access>, <https://nexteloud.bgc-jena.mpg.de/s/w2EiXdBDZmGX4F9>.

955 Forcing data to run the model for testbed simulations can be made available on request.

Competing interests. At least one of the (co-)authors is a member of the editorial board of Biogeosciences

Acknowledgement: KS acknowledges financial support from the IMPRS for Global Biogeochemical Cycles. [We thank Jan Engel and Julia Nabel for their technical assistance. We also thank Richard Norby and three anonymous referees whose comments greatly improved this paper.](#)

960

Contribution of authors. KS, KF and SZ designed the study. KS, KF and SZ interpreted the results. KS wrote model implementation and first draft of the manuscript. KF, AR, LY, MJ, BEM, SZ contributed to manuscript revision.

965

Additional Licences. Three figures were made ~~with~~using Biorender.com. The licenses can be found with the following links:

<https://biorender.com/4hh7q5e>

<https://biorender.com/w1lqfce>

<https://biorender.com/7hbj3d>

970 <https://biorender.com/b5hxuaa>

References

- 975 Ai, J., Banfield, C. C., Shao, G., Zamanian, K., Stürzebecher, T., Shi, L., Fan, L., Liu, X., Spielvogel, S., and Dippold, M. A.: What controls the availability of organic and inorganic P sources in top- and subsoils? A ³³P isotopic labeling study with root exudate addition, *Soil Biology and Biochemistry*, 185, 109129, <https://doi.org/10.1016/j.soilbio.2023.109129>, 2023.
- Akatsuki, M. and Makita, N.: Influence of fine root traits on in situ exudation rates in four conifers from different mycorrhizal associations, *Tree Physiology*, 40, 1071–1079, <https://doi.org/10.1093/treephys/tpaa051>, 2020.
- 980 Ataka, M., Sun, L., Nakaji, T., Katayama, A., and Hiura, T.: Five-year nitrogen addition affects fine root exudation and its correlation with root respiration in a dominant species, *Quercus crispula*, of a cool temperate forest, Japan, *Tree Physiology*, 40, 367–376, <https://doi.org/10.1093/treephys/tpz143>, 2020.
- Atkin, O. K., Meir, P., and Turnbull, M. H.: Improving representation of leaf respiration in large-scale predictive climate–vegetation models, *New Phytologist*, 202, 743–748, <https://doi.org/10.1111/nph.12686>, 2014.
- 985 Bastida, F., García, C., Fierer, N., Eldridge, D. J., Bowker, M. A., Abades, S., Alfaro, F. D., Asefaw Berhe, A., Cutler, N. A., Gallardo, A., García-Velázquez, L., Hart, S. C., Hayes, P. E., Hernández, T., Hseu, Z.-Y., Jehmlich, N., Kirchmair, M., Lambers, H., Neuhauser, S., Peña-Ramírez, V. M., Pérez, C. A., Reed, S. C., Santos, F., Siebe, C., Sullivan, B. W., Trivedi, P., Vera, A., Williams, M. A., Luis Moreno, J., and Delgado-Baquerizo, M.: Global ecological predictors of the soil priming effect, *Nat Commun*, 10, 3481, <https://doi.org/10.1038/s41467-019-11472-7>, 2019.
- 990 Brunn, M., Hafner, B. D., Zwetsloot, M. J., Weikl, F., Pritsch, K., Hikino, K., Ruehr, N. K., Sayer, E. J., and Bauerle, T. L.: Carbon allocation to root exudates is maintained in mature temperate tree species under drought, *New Phytologist*, 235, 965–977, <https://doi.org/10.1111/nph.18157>, 2022.
- Brunn, M., Mueller, C. W., Chari, N. R., Meier, I. C., Obersteiner, S., Phillips, R. P., Taylor, B., Tumber-Dávila, S. J., Ullah, S., and Klein, T.: Tree carbon allocation to root exudates: implications for carbon budgets, soil sequestration and drought response, *Tree Physiology*, 45, tpa026, <https://doi.org/10.1093/treephys/tpaf026>, 2025.
- 995 Castañeda-Gómez, L., Walker, J. K. M., Powell, J. R., Ellsworth, D. S., Pendall, E., and Carrillo, Y.: Impacts of elevated carbon dioxide on carbon gains and losses from soil and associated microbes in a *Eucalyptus* woodland, *Soil Biology and Biochemistry*, 143, 107734, <https://doi.org/10.1016/j.soilbio.2020.107734>, 2020.
- Chertov, O., Kuzyakov, Y., Pripulina, I., Frolov, P., Shanin, V., and Grabarnik, P.: Modelling the Rhizosphere Priming Effect in Combination with Soil Food Webs to Quantify Interaction between Living Plant, Soil Biota and Soil Organic Matter, *Plants*, 11, 2605, <https://doi.org/10.3390/plants11192605>, 2022.
- 1000 Cotrufo, M. F., Wallenstein, M. D., Boot, C. M., Deneff, K., and Paul, E.: The Microbial Efficiency-Matrix Stabilization (MEMS) framework integrates plant litter decomposition with soil organic matter stabilization: do labile plant inputs form stable soil organic matter?, *Global Change Biology*, 19, 988–995, <https://doi.org/10.1111/gcb.12113>, 2013.
- Crous, K. Y., Ósvaldsson, A., and Ellsworth, D. S.: Is phosphorus limiting in a mature *Eucalyptus* woodland? Phosphorus fertilisation stimulates stem growth, *Plant Soil*, 391, 293–305, <https://doi.org/10.1007/s11104-015-2426-4>, 2015.
- 1005 De Andrade, S. A. L., Borghi, A. A., De Oliveira, V. H., Gouveia, L. de M., Martins, A. P. I., and Mazzafera, P.: Phosphorus Shortage Induces an Increase in Root Exudation in Fifteen *Eucalypts* Species, *Agronomy*, 12, 2041, <https://doi.org/10.3390/agronomy12092041>, 2022.

- De Kauwe, M. G., Medlyn, B. E., Zaehle, S., Walker, A. P., Dietze, M. C., Wang, Y.-P., Luo, Y., Jain, A. K., El-Masri, B., Hickler, T., Wårlind, D., Weng, E., Parton, W. J., Thornton, P. E., Wang, S., Prentice, I. C., Asao, S., Smith, B., McCarthy, H. R., Iversen, C. M., Hanson, P. J., Warren, J. M., Oren, R., and Norby, R. J.: Where does the carbon go? A model–data intercomparison of vegetation carbon allocation and turnover processes at two temperate forest free-air CO₂ enrichment sites, *New Phytologist*, 203, 883–899, <https://doi.org/10.1111/nph.12847>, 2014.
- 1010 Dijkstra, F., Carrillo, Y., Pendall, E., and Morgan, J.: Rhizosphere priming: a nutrient perspective, *Frontiers in Microbiology*, 4, 2013.
- 1015 Drake, J. E., Gallet-Budynek, A., Hofmockel, K. S., Bernhardt, E. S., Billings, S. A., Jackson, R. B., Johnsen, K. S., Lichter, J., McCarthy, H. R., McCormack, M. L., Moore, D. J. P., Oren, R., Palmroth, S., Phillips, R. P., Phippen, J. S., Pritchard, S. G., Treseder, K. K., Schlesinger, W. H., DeLucia, E. H., and Finzi, A. C.: Increases in the flux of carbon belowground stimulate nitrogen uptake and sustain the long-term enhancement of forest productivity under elevated CO₂, *Ecology Letters*, 14, 349–357, <https://doi.org/10.1111/j.1461-0248.2011.01593.x>, 2011.
- 1020 Drake, J. E., Darby, B. A., Giasson, M.-A., Kramer, M. A., Phillips, R. P., and Finzi, A. C.: Stoichiometry constrains microbial response to root exudation- insights from a model and a field experiment in a temperate forest, *Biogeosciences*, 10, 821–838, <https://doi.org/10.5194/bg-10-821-2013>, 2013.
- Drake, J. E., Macdonald, C. A., Tjoelker, M. G., Crous, K. Y., Gimeno, T. E., Singh, B. K., Reich, P. B., Anderson, I. C., and Ellsworth, D. S.: Short-term carbon cycling responses of a mature eucalypt woodland to gradual stepwise enrichment of atmospheric CO₂ concentration, *Global Change Biology*, 22, 380–390, <https://doi.org/10.1111/gcb.13109>, 2016.
- 1025 Drake, J. E., Macdonald, C. A., Tjoelker, M. G., Reich, P. B., Singh, B. K., Anderson, I. C., and Ellsworth, D. S.: Three years of soil respiration in a mature eucalypt woodland exposed to atmospheric CO₂ enrichment, *Biogeochemistry*, 139, 85–101, <https://doi.org/10.1007/s10533-018-0457-7>, 2018.
- Du, E., Terrer, C., Pellegrini, A. F. A., Ahlström, A., van Lissa, C. J., Zhao, X., Xia, N., Wu, X., and Jackson, R. B.: Global patterns of terrestrial nitrogen and phosphorus limitation, *Nat. Geosci.*, 13, 221–226, <https://doi.org/10.1038/s41561-019-0530-4>, 2020.
- 1030 Ellsworth, D. S., Anderson, I. C., Crous, K. Y., Cooke, J., Drake, J. E., Gherlenda, A. N., Gimeno, T. E., Macdonald, C. A., Medlyn, B. E., Powell, J. R., Tjoelker, M. G., and Reich, P. B.: Elevated CO₂ does not increase eucalypt forest productivity on a low-phosphorus soil, *Nature Clim Change*, 7, 279–282, <https://doi.org/10.1038/nclimate3235>, 2017.
- 1035 Filion, M., Dutilleul, P., and Potvin, C.: Optimum experimental design for Free-Air Carbon dioxide Enrichment (FACE) studies, *Global Change Biology*, 6, 843–854, <https://doi.org/10.1046/j.1365-2486.2000.00353.x>, 2000.
- Fleischer, K., Rammig, A., De Kauwe, M. G., Walker, A. P., Domingues, T. F., Fuchslueger, L., Garcia, S., Goll, D. S., Grandis, A., Jiang, M., Haverd, V., Hofhansl, F., Holm, J. A., Kruijt, B., Leung, F., Medlyn, B. E., Mercado, L. M., Norby, R. J., Pak, B., von Randow, C., Quesada, C. A., Schaap, K. J., Valverde-Barrantes, O. J., Wang, Y.-P., Yang, X., Zaehle, S., Zhu, Q., and Lapola, D. M.: Amazon forest response to CO₂ fertilization dependent on plant phosphorus acquisition, *Nat. Geosci.*, 12, 736–741, <https://doi.org/10.1038/s41561-019-0404-9>, 2019.
- 1040 Friend, A. D. and Kiang, N. Y.: Land Surface Model Development for the GISS GCM: Effects of Improved Canopy Physiology on Simulated Climate, *Journal of Climate*, 18, 2883–2902, <https://doi.org/10.1175/JCLI3425.1>, 2005.
- 1045 van Groenigen, K. J., Qi, X., Osenberg, C. W., Luo, Y., and Hungate, B. A.: Faster Decomposition Under Increased Atmospheric CO₂ Limits Soil Carbon Storage, *Science*, 344, 508–509, <https://doi.org/10.1126/science.1249534>, 2014.

- van Groenigen, K. J., Osenberg, C. W., Terrer, C., Carrillo, Y., Dijkstra, F. A., Heath, J., Nie, M., Pendall, E., Phillips, R. P., and Hungate, B. A.: Faster turnover of new soil carbon inputs under increased atmospheric CO₂, *Global Change Biology*, 23, 4420–4429, <https://doi.org/10.1111/gcb.13752>, 2017.
- 1050 Hasegawa, S., Macdonald, C. A., and Power, S. A.: Elevated carbon dioxide increases soil nitrogen and phosphorus availability in a phosphorus-limited Eucalyptus woodland, *Global Change Biology*, 22, 1628–1643, <https://doi.org/10.1111/gcb.13147>, 2016.
- Hasegawa, S., Ryan, M. H., and Power, S. A.: CO₂ concentration and water availability alter the organic acid composition of root exudates in native Australian species, *Plant Soil*, 485, 507–524, <https://doi.org/10.1007/s11104-022-05845-z>, 2023.
- 1055 Hedley, M. J., Stewart, J. W. B., and Chauhan, B. S.: Changes in Inorganic and Organic Soil Phosphorus Fractions Induced by Cultivation Practices and by Laboratory Incubations, *Soil Science Society of America Journal*, 46, 970–976, <https://doi.org/10.2136/sssaj1982.03615995004600050017x>, 1982.
- Helfenstein, J., Ringeval, B., Tamburini, F., Mulder, V. L., Goll, D. S., He, X., Alblas, E., Wang, Y., Mollier, A., and Frossard, E.: Understanding soil phosphorus cycling for sustainable development: A review, *One Earth*, 7, 1727–1740, <https://doi.org/10.1016/j.oneear.2024.07.020>, 2024.
- 1060 Hinsinger, P.: Bioavailability of soil inorganic P in the rhizosphere as affected by root-induced chemical changes: a review, *Plant and Soil*, 237, 173–195, <https://doi.org/10.1023/A:1013351617532>, 2001.
- Jiang, M., Zaehle, S., De Kauwe, M. G., Walker, A. P., Caldararu, S., Ellsworth, D. S., and Medlyn, B. E.: The quasi-equilibrium framework revisited: analyzing long-term CO₂ enrichment responses in plant–soil models, *Geoscientific Model Development*, 12, 2069–2089, <https://doi.org/10.5194/gmd-12-2069-2019>, 2019.
- 1065 Jiang, M., Medlyn, B. E., Drake, J. E., Duursma, R. A., Anderson, I. C., Barton, C. V. M., Boer, M. M., Carrillo, Y., Castañeda-Gómez, L., Collins, L., Crous, K. Y., De Kauwe, M. G., dos Santos, B. M., Emmerson, K. M., Facey, S. L., Gherlenda, A. N., Gimeno, T. E., Hasegawa, S., Johnson, S. N., Kännaste, A., Macdonald, C. A., Mahmud, K., Moore, B. D., Nazaries, L., Neilson, E. H. J., Nielsen, U. N., Niinemets, Ü., Noh, N. J., Ochoa-Hueso, R., Pathare, V. S., Pendall, E., Pihlblad, J., Piñeiro, J., Powell, J. R., Power, S. A., Reich, P. B., Renchon, A. A., Riegler, M., Rinnan, R., Rymer, P. D., Salomón, R. L., Singh, B.
- 1070 K., Smith, B., Tjoelker, M. G., Walker, J. K. M., Wujeska-Klaue, A., Yang, J., Zaehle, S., and Ellsworth, D. S.: The fate of carbon in a mature forest under carbon dioxide enrichment, *Nature*, 580, 227–231, <https://doi.org/10.1038/s41586-020-2128-9>, 2020.
- Jiang, M., Medlyn, B. E., Wårlind, D., Knauer, J., Fleischer, K., Goll, D. S., Olin, S., Yang, X., Yu, L., Zaehle, S., Zhang, H., Lv, H., Crous, K. Y., Carrillo, Y., Macdonald, C., Anderson, I., Boer, M. M., Farrell, M., Gherlenda, A., Castañeda-Gómez, L., Hasegawa, S., Jarosch, K., Milham, P., Ochoa-Hueso, R., Pathare, V., Pihlblad, J., Nevado, J. P., Powell, J., Power, S. A., Reich, P., Riegler, M., Ellsworth, D. S., and Smith, B.: Carbon-phosphorus cycle models overestimate CO₂ enrichment response in a mature Eucalyptus forest, *Science Advances*, 10, ead15822, <https://doi.org/10.1126/sciadv.ad15822>, 2024a.
- 1075 Jiang, M., Crous, K. Y., Carrillo, Y., Macdonald, C. A., Anderson, I. C., Boer, M. M., Farrell, M., Gherlenda, A. N., Castañeda-Gómez, L., Hasegawa, S., Jarosch, K., Milham, P. J., Ochoa-Hueso, R., Pathare, V., Pihlblad, J., Piñeiro, J., Powell, J. R., Power, S. A., Reich, P. B., Riegler, M., Zaehle, S., Smith, B., Medlyn, B. E., and Ellsworth, D. S.: Microbial competition for phosphorus limits the CO₂ response of a mature forest, *Nature*, 1–6, <https://doi.org/10.1038/s41586-024-07491-0>, 2024b.
- 1080 Jiang, Z., Thakur, M. P., Liu, R., Zhou, G., Zhou, L., Fu, Y., Zhang, P., He, Y., Shao, J., Gao, J., Li, N., Wang, X., Jia, S., Chen, Y., Zhang, C., and Zhou, X.: Soil P availability and mycorrhizal type determine root exudation in sub-tropical forests, *Soil Biology and Biochemistry*, 171, 108722, <https://doi.org/10.1016/j.soilbio.2022.108722>, 2022.

- 1085 Johansson, E. M., Fransson, P. M. A., Finlay, R. D., and van Hees, P. A. W.: Quantitative analysis of soluble exudates produced by ectomycorrhizal roots as a response to ambient and elevated CO₂, *Soil Biology and Biochemistry*, 41, 1111–1116, <https://doi.org/10.1016/j.soilbio.2009.02.016>, 2009.
- Jones, D. L., Hodge, A., and Kuzyakov, Y.: Plant and mycorrhizal regulation of rhizodeposition, *New Phytologist*, 163, 459–480, <https://doi.org/10.1111/j.1469-8137.2004.01130.x>, 2004.
- 1090 Kästner, M., Miltner, A., Thiele-Bruhn, S., and Liang, C.: Microbial Necromass in Soils—Linking Microbes to Soil Processes and Carbon Turnover, *Front. Environ. Sci.*, 9, <https://doi.org/10.3389/fenvs.2021.756378>, 2021.
- Kull, O. and Kruijt, B.: Leaf photosynthetic light response: a mechanistic model for scaling photosynthesis to leaves and canopies, *Functional Ecology*, 12, 767–777, <https://doi.org/10.1046/j.1365-2435.1998.00257.x>, 1998.
- 1095 Kuzyakov, Y., Horwath, W. R., Dorodnikov, M., and Blagodatskaya, E.: Review and synthesis of the effects of elevated atmospheric CO₂ on soil processes: No changes in pools, but increased fluxes and accelerated cycles, *Soil Biol. Biochem.*, 128, 66–78, <https://doi.org/10.1016/j.soilbio.2018.10.005>, 2019.
- Lambers, H.: Phosphorus Acquisition and Utilization in Plants, *Annu. Rev. Plant Biol.*, 73, 17–42, <https://doi.org/10.1146/annurev-arplant-102720-125738>, 2022.
- 1100 Leuschner, C., Tückmantel, T., and Meier, I. C.: Temperature effects on root exudation in mature beech (*Fagus sylvatica* L.) forests along an elevational gradient, *Plant Soil*, <https://doi.org/10.1007/s11104-022-05629-5>, 2022.
- Li, Z., Liu, Z., Gao, G., Yang, X., and Gu, J.: Shift from Acquisitive to Conservative Root Resource Acquisition Strategy Associated with Increasing Tree Age: A Case Study of *Fraxinus mandshurica*, *Forests*, 12, 1797, <https://doi.org/10.3390/f12121797>, 2021.
- 1105 Liang, C., Schimel, J. P., and Jastrow, J. D.: The importance of anabolism in microbial control over soil carbon storage, *Nat Microbiol*, 2, 1–6, <https://doi.org/10.1038/nmicrobiol.2017.105>, 2017.
- Liang, C., Amelung, W., Lehmann, J., and Kästner, M.: Quantitative assessment of microbial necromass contribution to soil organic matter, *Global Change Biology*, 25, 3578–3590, <https://doi.org/10.1111/gcb.14781>, 2019.
- Lloyd, J. and Taylor, J. A.: On the Temperature Dependence of Soil Respiration, *Functional Ecology*, 8, 315, <https://doi.org/10.2307/2389824>, 1994.
- 1110 Lopez-Sangil, L., George, C., Medina-Barcenas, E., Birkett, A. J., Baxendale, C., Bréchet, L. M., Estradera-Gumbau, E., and Sayer, E. J.: The Automated Root Exudate System (ARES): a method to apply solutes at regular intervals to soils in the field, *Methods in Ecology and Evolution*, 8, 1042–1050, <https://doi.org/10.1111/2041-210X.12764>, 2017.
- Manzoni, S., Taylor, P., Richter, A., Porporato, A., and Ågren, G. I.: Environmental and stoichiometric controls on microbial carbon-use efficiency in soils, *New Phytologist*, 196, 79–91, <https://doi.org/10.1111/j.1469-8137.2012.04225.x>, 2012.
- 1115 Margalef, O., Sardans, J., Fernández-Martínez, M., Molowny-Horas, R., Janssens, I. A., Ciais, P., Goll, D., Richter, A., Obersteiner, M., Asensio, D., and Peñuelas, J.: Global patterns of phosphatase activity in natural soils, *Sci Rep*, 7, 1337, <https://doi.org/10.1038/s41598-017-01418-8>, 2017.
- Marklein, A. R. and Houlton, B. Z.: Nitrogen inputs accelerate phosphorus cycling rates across a wide variety of terrestrial ecosystems, *New Phytologist*, 193, 696–704, <https://doi.org/10.1111/j.1469-8137.2011.03967.x>, 2012.

- 1120 McGill, W. B. and Cole, C. V.: Comparative aspects of cycling of organic C, N, S and P through soil organic matter, *Geoderma*, 26, 267–286, [https://doi.org/10.1016/0016-7061\(81\)90024-0](https://doi.org/10.1016/0016-7061(81)90024-0), 1981.
- Medlyn, B. E., De Kauwe, M. G., Zaehle, S., Walker, A. P., Duursma, R. A., Luus, K., Mishurov, M., Pak, B., Smith, B., Wang, Y.-P., Yang, X., Crous, K. Y., Drake, J. E., Gimeno, T. E., Macdonald, C. A., Norby, R. J., Power, S. A., Tjoelker, M. G., and Ellsworth, D. S.: Using models to guide field experiments: a priori predictions for the CO₂ response of a nutrient- and water-limited native Eucalypt woodland, *Global Change Biology*, 22, 2834–2851, <https://doi.org/10.1111/gcb.13268>, 2016.
- 1125 Meier, I. C., Tückmantel, T., Heitkötter, J., Müller, K., Preusser, S., Wrobel, T. J., Kandeler, E., Marschner, B., and Leuschner, C.: Root exudation of mature beech forests across a nutrient availability gradient: the role of root morphology and fungal activity, *New Phytologist*, 226, 583–594, <https://doi.org/10.1111/nph.16389>, 2020.
- Nannipieri, P., Giagnoni, L., Landi, L., and Renella, G.: Role of Phosphatase Enzymes in Soil, in: *Phosphorus in Action: Biological Processes in Soil Phosphorus Cycling*, edited by: Bünemann, E., Oberson, A., and Frossard, E., Springer, Berlin, Heidelberg, 215–243, https://doi.org/10.1007/978-3-642-15271-9_9, 2011.
- 1130 Norby, R. J.: Forest productivity response to elevated CO₂ in free-air CO₂ enrichment experiments: the 23 percent solution, revisited, *New Phytologist*, <https://doi.org/10.1111/nph.70162>, 2025.
- Norby, R. J., Warren, J. M., Iversen, C. M., Medlyn, B. E., and McMurtrie, R. E.: CO₂ enhancement of forest productivity constrained by limited nitrogen availability, *Proceedings of the National Academy of Sciences*, 107, 19368–19373, <https://doi.org/10.1073/pnas.1006463107>, 2010.
- 1135 Norby, R. J., Loader, N. J., Mayoral, C., Ullah, S., Curioni, G., Smith, A. R., Reay, M. K., van Wijngaarden, K., Amjad, M. S., Brettle, D., Crockatt, M. E., Denny, G., Grzesik, R. T., Hamilton, R. L., Hart, K. M., Hartley, I. P., Jones, A. G., Kourmouli, A., Larsen, J. R., Shi, Z., Thomas, R. M., and MacKenzie, A. R.: Enhanced woody biomass production in a mature temperate forest under elevated CO₂, *Nat. Clim. Chang.*, 14, 983–988, <https://doi.org/10.1038/s41558-024-02090-3>, 2024.
- Ochoa-Hueso, R., Hughes, J., Delgado-Baquerizo, M., Drake, J. E., Tjoelker, M. G., Piñeiro, J., and Power, S. A.: Rhizosphere-driven increase in nitrogen and phosphorus availability under elevated atmospheric CO₂ in a mature Eucalyptus woodland, *Plant Soil*, 416, 283–295, <https://doi.org/10.1007/s11104-017-3212-2>, 2017.
- Phillips, R. P., ERLITZ, Y., Bier, R., and Bernhardt, E. S.: New approach for capturing soluble root exudates in forest soils, *Functional Ecology*, 22, 990–999, <https://doi.org/10.1111/j.1365-2435.2008.01495.x>, 2008.
- 1145 Phillips, R. P., Finzi, A. C., and Bernhardt, E. S.: Enhanced root exudation induces microbial feedbacks to N cycling in a pine forest under long-term CO₂ fumigation, *Ecology Letters*, 14, 187–194, <https://doi.org/10.1111/j.1461-0248.2010.01570.x>, 2011.
- Pihlblad, J., Andresen, L. C., Macdonald, C. A., Ellsworth, D. S., and Carrillo, Y.: The influence of elevated CO₂ and soil depth on rhizosphere activity and nutrient availability in a mature *Eucalyptus* woodland, *Biogeosciences*, 20, 505–521, <https://doi.org/10.5194/bg-20-505-2023>, 2023.
- 1150 Piñeiro, J., Ochoa-Hueso, R., Drake, J. E., Tjoelker, M. G., and Power, S. A.: Water availability drives fine root dynamics in a Eucalyptus woodland under elevated atmospheric CO₂ concentration, *Functional Ecology*, 34, 2389–2402, <https://doi.org/10.1111/1365-2435.13660>, 2020.
- 1155 Piñeiro, J., Ochoa-Hueso, R., Serrano-Grijalva, L., and Power, S. A.: Phosphorus and water supply independently control productivity and soil enzyme activity responses to elevated CO₂ in an understorey community from a Eucalyptus woodland, *Plant Soil*, 483, 643–657, <https://doi.org/10.1007/s11104-022-05763-0>, 2023.

- Prescott, C. E., Grayston, S. J., Helmisaari, H.-S., Kaštovská, E., Körner, C., Lambers, H., Meier, I. C., Millard, P., and Ostonen, I.: Surplus Carbon Drives Allocation and Plant–Soil Interactions, *Trends in Ecology & Evolution*, 35, 1110–1118, <https://doi.org/10.1016/j.tree.2020.08.007>, 2020.
- 1160 Reay, M. K., Sayer, E. J., Smith, A., Pastor, V., Kourmouli, A., Marshall, M., Grzesik, R. T., Evans, I., Rumeau, M., Hart, K., Ma, J., Norby, R. J., MacKenzie, A. R., Hamilton, R. L., Hartley, I. P., and Ullah, S.: Elevated CO₂ alters relative belowground carbon investment for nutrient acquisition in a mature temperate forest, *Proceedings of the National Academy of Sciences*, 122, e2503595122, <https://doi.org/10.1073/pnas.2503595122>, 2025.
- 1165 Reichert, T., Rammig, A., Fuchsluger, L., Lugli, L. F., Quesada, C. A., and Fleischer, K.: Plant phosphorus-use and -acquisition strategies in Amazonia, *New Phytologist*, 234, 1126–1143, <https://doi.org/10.1111/nph.17985>, 2022.
- Ross, G. M., Horn, S., Macdonald, C. A., Powell, J. R., Reynolds, J. K., Ryan, M. M., Cook, J. M., and Nielsen, U. N.: Metabarcoding mites: Three years of elevated CO₂ has no effect on oribatid assemblages in a *Eucalyptus* woodland, *Pedobiologia*, 81–82, 150667, <https://doi.org/10.1016/j.pedobi.2020.150667>, 2020.
- 1170 Rumeau, M., Pihlblad, J., Sgouridis, F., Fereday, G., Reay, M. K., Carrillo, Y., Hartley, I. P., Sayer, E., Hamilton, L., Mackenzie, A. R., and Ullah, S.: Root exudate stoichiometry is a key driver of soil N cycling: implications for forest responses to global change, *Soil Biology and Biochemistry*, 208, 109856, <https://doi.org/10.1016/j.soilbio.2025.109856>, 2025.
- Schimel, J. P. and Weintraub, M. N.: The implications of exoenzyme activity on microbial carbon and nitrogen limitation in soil: a theoretical model, *Soil Biology and Biochemistry*, 35, 549–563, [https://doi.org/10.1016/S0038-0717\(03\)00015-4](https://doi.org/10.1016/S0038-0717(03)00015-4), 2003.
- 1175 Sistla, S. A., Rastetter, E. B., and Schimel, J. P.: Responses of a tundra system to warming using SCAMPS: a stoichiometrically coupled, acclimating microbe–plant–soil model, *Ecological Monographs*, 84, 151–170, <https://doi.org/10.1890/12-2119.1>, 2014.
- Sokol, N. W., Kuebbing, Sara E., Karlsen-Ayala, E., and Bradford, M. A.: Evidence for the primacy of living root inputs, not root or shoot litter, in forming soil organic carbon, *New Phytologist*, 221, 233–246, <https://doi.org/10.1111/nph.15361>, 2019.
- 1180 Spohn, M.: Microbial respiration per unit microbial biomass depends on litter layer carbon-to-nitrogen ratio, *Biogeosciences*, 12, 817–823, <https://doi.org/10.5194/bg-12-817-2015>, 2015.
- Spohn, M., Ermak, A., and Kuzyakov, Y.: Microbial gross organic phosphorus mineralization can be stimulated by root exudates – A ³³P isotopic dilution study, *Soil Biology and Biochemistry*, 65, 254–263, <https://doi.org/10.1016/j.soilbio.2013.05.028>, 2013.
- 1185 Spohn, M., Klaus, K., Wanek, W., and Richter, A.: Microbial carbon use efficiency and biomass turnover times depending on soil depth – Implications for carbon cycling, *Soil Biology and Biochemistry*, 96, 74–81, <https://doi.org/10.1016/j.soilbio.2016.01.016>, 2016.
- Su, Y., Xu, G., Lu, X., Jiang, H., Peng, S., Zhao, H., Liu, M., and Duan, B.: Interactive effects of citric acid and mineral fertilization on soil microbial carbon use efficiency in the rhizosphere of two coniferous species, *European Journal of Soil Biology*, 112, 103428, <https://doi.org/10.1016/j.ejsobi.2022.103428>, 2022.
- 1190 Sun, L., Kominami, Y., Yoshimura, K., and Kitayama, K.: Root-exudate flux variations among four co-existing canopy species in a temperate forest, Japan, *Ecological Research*, 32, 331–339, <https://doi.org/10.1007/s11284-017-1440-9>, 2017.

- 1195 Sun, L., Ataka, M., Han, M., Han, Y., Gan, D., Xu, T., Guo, Y., and Zhu, B.: Root exudation as a major competitive fine-root functional trait of 18 coexisting species in a subtropical forest, *New Phytologist*, 229, 259–271, <https://doi.org/10.1111/nph.16865>, 2021.
- 1200 Sun, Z., Liu, S., Zhang, T., Zhao, X., Chen, S., and Wang, Q.: Priming of soil organic carbon decomposition induced by exogenous organic carbon input: a meta-analysis, *Plant Soil*, 443, 463–471, <https://doi.org/10.1007/s11104-019-04240-5>, 2019.
- Talbot, J. M., Allison, S. D., and Treseder, K. K.: Decomposers in disguise: mycorrhizal fungi as regulators of soil C dynamics in ecosystems under global change, *Functional Ecology*, 22, 955–963, <https://doi.org/10.1111/j.1365-2435.2008.01402.x>, 2008.
- Taneva, L., Pippen, J. S., Schlesinger, W. H., and Gonzalez-Meler, M. A.: The turnover of carbon pools contributing to soil CO₂ and soil respiration in a temperate forest exposed to elevated CO₂ concentration, *Global Change Biology*, 12, 983–994, <https://doi.org/10.1111/j.1365-2486.2006.01147.x>, 2006.
- 1205 Tang, J. Y. and Riley, W. J.: A total quasi-steady-state formulation of substrate uptake kinetics in complex networks and an example application to microbial litter decomposition, *Biogeosciences*, 10, 8329–8351, <https://doi.org/10.5194/bg-10-8329-2013>, 2013.
- 1210 Tao, F., Huang, Y., Hungate, B. A., Manzoni, S., Frey, S. D., Schmidt, M. W. I., Reichstein, M., Carvalhais, N., Ciais, P., Jiang, L., Lehmann, J., Wang, Y.-P., Houlton, B. Z., Ahrens, B., Mishra, U., Hugelius, G., Hocking, T. D., Lu, X., Shi, Z., Viatkin, K., Vargas, R., Yigini, Y., Omuto, C., Malik, A. A., Peralta, G., Cuevas-Corona, R., Di Paolo, L. E., Luotto, I., Liao, C., Liang, Y.-S., Saynes, V. S., Huang, X., and Luo, Y.: Microbial carbon use efficiency promotes global soil carbon storage, *Nature*, 618, 981–985, <https://doi.org/10.1038/s41586-023-06042-3>, 2023.
- 1215 Tao, J., Riley, W., Tang, J., Zhu, Q., Pegoraro, E., Castanha, C., Abramoff, R., Torn, M., Tao, J., Riley, W., Tang, J., Zhu, Q., Pegoraro, E., Castanha, C., Abramoff, R., and Torn, M.: Representing Soil Microbial Dynamics and Organo-Mineral Interactions in the E3SM Land Model (ELM-ReSOM), *Journal of Advances in Modeling Earth Systems*, 17, <https://doi.org/10.1029/2024ms004874>, 2025.
- Terrer, C., Vicca, S., Hungate, B. A., Phillips, R. P., and Prentice, I. C.: Mycorrhizal association as a primary control of the CO₂ fertilization effect, *Science*, 353, 72–74, <https://doi.org/10.1126/science.aaf4610>, 2016.
- 1220 Terrer, C., Phillips, R. P., Hungate, B. A., Rosende, J., Pett-Ridge, J., Craig, M. E., van Groenigen, K. J., Keenan, T. F., Sulman, B. N., Stocker, B. D., Reich, P. B., Pellegrini, A. F. A., Pendall, E., Zhang, H., Evans, R. D., Carrillo, Y., Fisher, J. B., Van Sundert, K., Vicca, S., and Jackson, R. B.: A trade-off between plant and soil carbon storage under elevated CO₂, *Nature*, 591, 599–603, <https://doi.org/10.1038/s41586-021-03306-8>, 2021.
- 1225 Thum, T., Caldararu, S., Engel, J., Kern, M., Pallandt, M., Schnur, R., Yu, L., and Zaehle, S.: A new model of the coupled carbon, nitrogen, and phosphorus cycles in the terrestrial biosphere (QUINCY v1.0; revision 1996), *Geoscientific Model Development*, 12, 4781–4802, <https://doi.org/10.5194/gmd-12-4781-2019>, 2019.
- Thurner, M. A., Caldararu, S., Engel, J., Rammig, A., and Zaehle, S.: Modelled forest ecosystem carbon-nitrogen dynamics with integrated mycorrhizal processes under elevated CO₂, *Biogeosciences Discussions*, 1–30, <https://doi.org/10.5194/bg-2023-109>, 2023.
- 1230 Turner, B. L., Wells, A., and Condron, L. M.: Soil organic phosphorus transformations along a coastal dune chronosequence under New Zealand temperate rain forest, *Biogeochemistry*, 121, 595–611, <https://doi.org/10.1007/s10533-014-0025-8>, 2014.

- Vestergård, M., Reinsch, S., Bengtson, P., Ambus, P., and Christensen, S.: Enhanced priming of old, not new soil carbon at elevated atmospheric CO₂, *Soil Biology and Biochemistry*, 100, 140–148, <https://doi.org/10.1016/j.soilbio.2016.06.010>, 2016.
- 1235 Walker, A. P., Zaehle, S., Medlyn, B. E., De Kauwe, M. G., Asao, S., Hickler, T., Parton, W., Ricciuto, D. M., Wang, Y.-P., Wårlind, D., and Norby, R. J.: Predicting long-term carbon sequestration in response to CO₂ enrichment: How and why do current ecosystem models differ?, *Global Biogeochemical Cycles*, 29, 476–495, <https://doi.org/10.1002/2014GB004995>, 2015.
- 1240 Walker, A. P., De Kauwe, M. G., Medlyn, B. E., Zaehle, S., Iversen, C. M., Asao, S., Guenet, B., Harper, A., Hickler, T., Hungate, B. A., Jain, A. K., Luo, Y., Lu, X., Lu, M., Luus, K., Megonigal, J. P., Oren, R., Ryan, E., Shu, S., Talhelm, A., Wang, Y.-P., Warren, J. M., Werner, C., Xia, J., Yang, B., Zak, D. R., and Norby, R. J.: Decadal biomass increment in early secondary succession woody ecosystems is increased by CO₂ enrichment, *Nat Commun*, 10, 454, <https://doi.org/10.1038/s41467-019-08348-1>, 2019.
- 1245 Walker, A. P., De Kauwe, M. G., Bastos, A., Belmecheri, S., Georgiou, K., Keeling, R. F., McMahon, S. M., Medlyn, B. E., Moore, D. J. P., Norby, R. J., Zaehle, S., Anderson-Teixeira, K. J., Battipaglia, G., Brienen, R. J. W., Cabugao, K. G., Cailleret, M., Campbell, E., Canadell, J. G., Ciais, P., Craig, M. E., Ellsworth, D. S., Farquhar, G. D., Faticchi, S., Fisher, J. B., Frank, D. C., Graven, H., Gu, L., Haverd, V., Heilman, K., Heimann, M., Hungate, B. A., Iversen, C. M., Joos, F., Jiang, M., Keenan, T. F., Knauer, J., Körner, C., Leshyk, V. O., Leuzinger, S., Liu, Y., MacBean, N., Malhi, Y., McVicar, T. R., Penuelas, J., Pongratz, J., Powell, A. S., Riutta, T., Sabot, M. E. B., Schleucher, J., Sitch, S., Smith, W. K., Sulman, B., Taylor, B., Terrer, C., Torn, M. S., Treseder, K. K., Trugman, A. T., Trumbore, S. E., van Mantgem, P. J., Voelker, S. L., Whelan, M. E., and Zuidema, P. A.: Integrating the evidence for a terrestrial carbon sink caused by increasing atmospheric CO₂, *New Phytologist*, 1250, 229, 2413–2445, <https://doi.org/10.1111/nph.16866>, 2021.
- Walker, T. W. and Syers, J. K.: The fate of phosphorus during pedogenesis, *Geoderma*, 15, 1–19, [https://doi.org/10.1016/0016-7061\(76\)90066-5](https://doi.org/10.1016/0016-7061(76)90066-5), 1976.
- Wang, Y. and Lambers, H.: Root-released organic anions in response to low phosphorus availability: recent progress, challenges and future perspectives, *Plant Soil*, 447, 135–156, <https://doi.org/10.1007/s11104-019-03972-8>, 2020.
- 1255 Wang, Y.-P., Huang, Y., Augusto, L., Goll, D. S., Helfenstein, J., and Hou, E.: Toward a Global Model for Soil Inorganic Phosphorus Dynamics: Dependence of Exchange Kinetics and Soil Bioavailability on Soil Physicochemical Properties, *Global Biogeochemical Cycles*, 36, e2021GB007061, <https://doi.org/10.1029/2021GB007061>, 2022.
- Wen, Z., White, P. J., Shen, J., and Lambers, H.: Linking root exudation to belowground economic traits for resource acquisition, *New Phytologist*, 233, 1620–1635, <https://doi.org/10.1111/nph.17854>, 2022.
- 1260 Wieder, W. R., Cleveland, C. C., Smith, W. K., and Todd-Brown, K.: Future productivity and carbon storage limited by terrestrial nutrient availability, *Nature Geosci*, 8, 441–444, <https://doi.org/10.1038/ngeo2413>, 2015.
- Wutzler, T., Zaehle, S., Schrumph, M., Ahrens, B., and Reichstein, M.: Adaptation of microbial resource allocation affects modelled long term soil organic matter and nutrient cycling, *Soil Biology and Biochemistry*, 115, 322–336, <https://doi.org/10.1016/j.soilbio.2017.08.031>, 2017.
- 1265 Wutzler, T., Yu, L., Schrumph, M., and Zaehle, S.: Simulating long-term responses of soil organic matter turnover to substrate stoichiometry by abstracting fast and small-scale microbial processes: the Soil Enzyme Steady Allocation Model (SESAM; v3.0), *Geoscientific Model Development*, 15, 8377–8393, <https://doi.org/10.5194/gmd-15-8377-2022>, 2022.

- 1270 Yin, H., Li, Y., Xiao, J., Xu, Z., Cheng, X., and Liu, Q.: Enhanced root exudation stimulates soil nitrogen transformations in a subalpine coniferous forest under experimental warming, *Global Change Biology*, 19, 2158–2167, <https://doi.org/10.1111/gcb.12161>, 2013.
- Yu, L., Ahrens, B., Wutzler, T., Schrumpf, M., and Zaehle, S.: Jena Soil Model (JSM v1.0; revision 1934): a microbial soil organic carbon model integrated with nitrogen and phosphorus processes, *Geoscientific Model Development*, 13, 783–803, <https://doi.org/10.5194/gmd-13-783-2020>, 2020.
- 1275 Yu, L., Caldararu, S., Ahrens, B., Wutzler, T., Schrumpf, M., Helfenstein, J., Pistocchi, C., and Zaehle, S.: Improved representation of phosphorus exchange on soil mineral surfaces reduces estimates of phosphorus limitation in temperate forest ecosystems, *Biogeosciences*, 20, 57–73, <https://doi.org/10.5194/bg-20-57-2023>, 2023.
- 1280 Zaehle, S., Medlyn, B. E., De Kauwe, M. G., Walker, A. P., Dietze, M. C., Hickler, T., Luo, Y., Wang, Y.-P., El-Masri, B., Thornton, P., Jain, A., Wang, S., Warlind, D., Weng, E., Parton, W., Iversen, C. M., Gallet-Budynek, A., McCarthy, H., Finzi, A., Hanson, P. J., Prentice, I. C., Oren, R., and Norby, R. J.: Evaluation of 11 terrestrial carbon–nitrogen cycle models against observations from two temperate Free-Air CO₂ Enrichment studies, *New Phytologist*, 202, 803–822, <https://doi.org/10.1111/nph.12697>, 2014.
- Zerihun, A., McKENZIE, B. A., and Morton, J. D.: Photosynthate costs associated with the utilization of different nitrogen–forms: influence on the carbon balance of plants and shoot–root biomass partitioning, *New Phytologist*, 138, 1–11, <https://doi.org/10.1046/j.1469-8137.1998.00893.x>, 1998.
- 1285 Zhang, C., Cai, Y., Zhang, T., He, T., Li, J., Li, X., and Zhao, Q.: Litter removal increases the plant carbon input to soil in a *Pinus massoniana* plantation, *Eur J Forest Res*, 141, 833–843, <https://doi.org/10.1007/s10342-022-01476-2>, 2022.
- Zhang, H., Goll, D. S., Wang, Y.-P., Ciais, P., Wieder, W. R., Abramoff, R., Huang, Y., Guenet, B., Prescher, A.-K., Viscarra Rossel, R. A., Barré, P., Chenu, C., Zhou, G., and Tang, X.: Microbial dynamics and soil physicochemical properties explain large-scale variations in soil organic carbon, *Global Change Biology*, 26, 2668–2685, <https://doi.org/10.1111/gcb.14994>, 2020.
- 1290 Zhang, Z., Qiao, M., Li, D., Yin, H., and Liu, Q.: Do warming-induced changes in quantity and stoichiometry of root exudation promote soil N transformations via stimulation of soil nitrifiers, denitrifiers and ammonifiers?, *European Journal of Soil Biology*, 74, 60–68, <https://doi.org/10.1016/j.ejsobi.2016.03.007>, 2016.
- 1295 Zhou, J., Wen, Y., Shi, L., Marshall, M. R., Kuzyakov, Y., Blagodatskaya, E., and Zang, H.: Strong priming of soil organic matter induced by frequent input of labile carbon, *Soil Biology and Biochemistry*, 152, 108069, <https://doi.org/10.1016/j.soilbio.2020.108069>, 2021.